On Merger of Axion Dark Matter Clumps and Parametric Resonance of Photons

inspirehep.net/literature/1794475 - inspirehep.net/literature/1776696
inspirehep.net/literature/1670964 - inspirehep.net/literature/1668954
inspirehep.net/literature/1630599

Online "Newton 1665" seminars – phenomenology/theory/astro/cosmo

JYVÄSKYLÄN YLIOPISTO
UNIVERSITY OF JYVÄSKYLÄ

HELSINKI INSTITUTE OF PHYSICS

Enrico D. Schiappacasse

July 2nd, 2020

OUTLINE

- INTRODUCTION
  - Axion Searches
  - Axion Clumps Formation
- AXIONS AND PHOTONS
  - Axion Field Theory
  - Axion Dark Matter Clumps
  - Axions and Photons
- AXION STAR MERGER
  - Numerical setup
  - (Non-) Head-on collision between two ground state axion star
  - Parameter Space for merger
- ASTROPHYSICAL SIGNATURES VIA RESONANT PHOTON EMISSION
  - Collision and Merger rate for axion stars
  - Photon Emission
  - Detectability
- DISCUSSION

INTRODUCTION

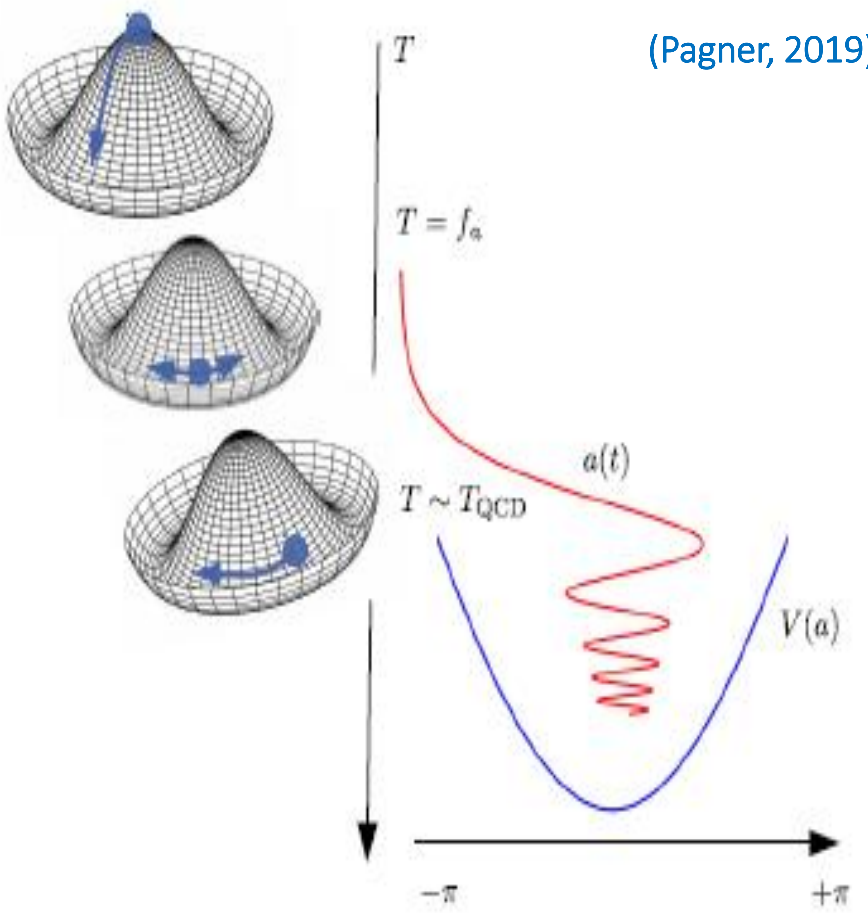

- A wide range of astrophysical observations are well explained by including cold dark matter (CDM) (Peebles, 2015).

- A popular dark matter candidate is the QCD axion: PG-boson associated with SSB of $U(1)_{PQ}$, which was introduced as a possible solution of the strong CP problem (Peccei and Quinn, 1977) .

- The axion field acquires a mass after the QCD phase transition, and then begin to act as a form of CDM (Preskill et al. 1983).

- Extensively axion searching in recent years

- Haloscopes (ADMX ColL. 2018) and Heliscopes (Armengaud et al. 2014)
- Oscillating electric dipole moment (Graham & Rajendran, 2011)
- Atomic and molecular transitions (Sikivie 2014)
- Indirect Axion searches (Iwasaki 2015; Hook et al. 2018)

- Many of these searches exploit the axion-photon coupling

$$\Delta\mathcal{L} = g_{\phi\gamma\gamma}\phi \boldsymbol{E}\cdot\boldsymbol{B}$$

- Ground based experiments as ADMX (Asztalo et al. 2010)
- Photon emisión by collisions of axion clumps and neutron stars (Iwazaki 2015)

- A NOVEL SCENARIO

A portion of axions may organize into gravitationally bound clumps and be present in large number in the galaxy today.

For moderate $g_{\phi\gamma\gamma}$ clumps with $M > M_c^*$ may undergo parametric resonance of photons

To have clumps above the critical mass (M_c^*) in the galaxy today would require mergers.

The output of cohererent radiowaves may potentially be detected on the Earth.

- Bose-Einstein Condensate (BEC) of axions known as "Axion stars" or "Clumps" or "Bose Stars"
- GRAVITY + SELF-INTERACTION + KINETIC PRESSURE

Stable Configurations in the non-relativistic regime

- Axion Clump formation would depend on the scenario at which the PQ-symmetry is broken

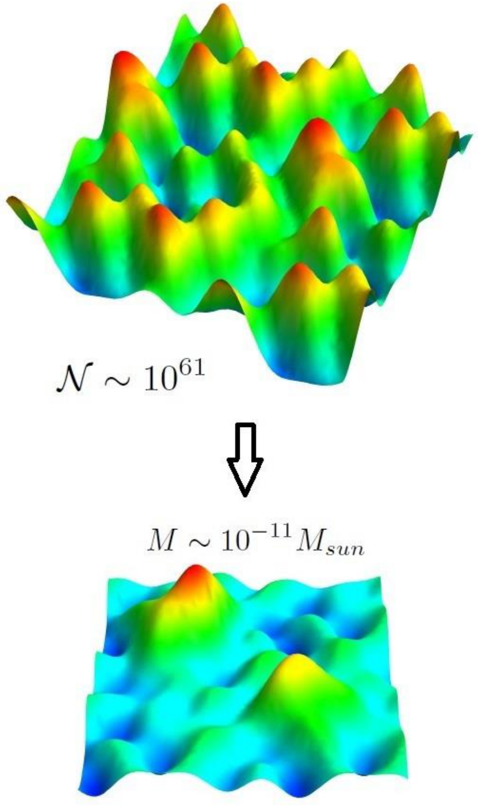

(Guth, M.H., Prescod-Weinstein, 2015)

Broken after inflation

- The axion field remain inhomogeneous from one Hubble patch to the next.
- Strong mode-mode gravitational interactions lead to BEC formation.
- We need to assume $N_{DW} = 1$ (KSVZ model) to avoid domain-wall problem

$$10^9\mathrm{GeV} < F_a < 10^{11}\mathrm{GeV}$$

(Kawasaki et. al 2015)

- The axion field is driven to be highly homogeneous on large scales → Unclear if it may form a BEC in the late Universe.
- Axion clumps may kinetically nucleate in dark mini-halos around PBHs (Hertzberg, Schiappacasse, Yanagida 2020).
- Axion-like particles clumps may form via tachyonic instability (Fukunaga et al., 2020)

$$\Omega_\phi h^2 \sim 0.7 \left(\frac{F_a}{10^{12}\mathrm{GeV}}\right)^{7/6} \left(\frac{\Theta_i}{\pi}\right)^2 \rightarrow 10^9\mathrm{GeV} < F_a < 10^{17}\mathrm{GeV}$$

Broken before inflation

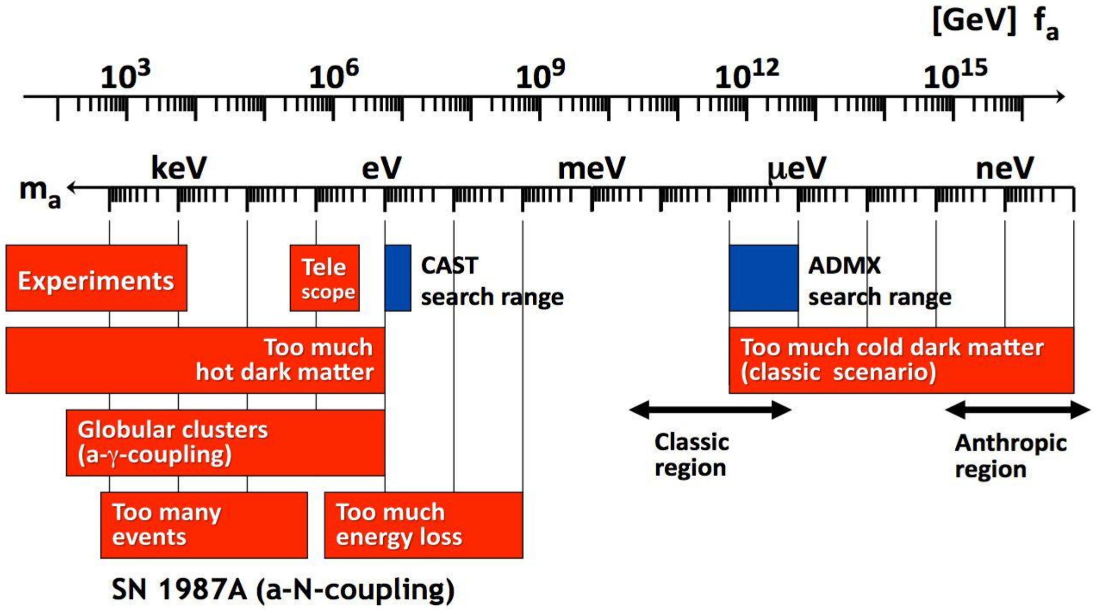

AXION FIELD THEORY

- In the effective theory for axions, they can be described by a real scalar field $\phi(x,t)$ with a small potential $V(\phi)$ coming from nonperturbative QCD effects:

$$\mathcal{L} = \sqrt{-g}\left[\frac{R}{16\pi G_N} + g^{\mu\nu}\nabla_\mu\phi\nabla_\nu\phi - V(\phi)\right]$$

- Expanding around the CP preserving vacuum: $V(\phi) = \frac{1}{2}m_\phi^2\phi^2 + \frac{\lambda}{4!}\phi^4 + \mathcal{O}(\phi^6)$

$$\lambda = -\gamma\frac{m_\phi^2}{F_a^2}$$

$\gamma = 1$: $V(\phi) = m_\phi^2 f_a^2[1-\cos(\phi/f_a)]$

$\gamma = 1 - 3m_u m_d/(m_u + m_d)^2 \approx 0.3$ (Grilli et al., 2016)

- For the standard QCD axion (Weinberg, 1978) :

$$m_\phi\left(m_{u,d,\pi}, f_\pi, f_a\right) \backsimeq 10^{-5}\mathrm{eV}\left(\frac{6\cdot 10^{11}\mathrm{GeV}}{F_a}\right)$$

- In the non-relativistic regime we can rewrite the real axion field in terms of a complex Schrodinger field ψ

$$\phi(\boldsymbol{x},t)=\frac{1}{\sqrt{2m_\phi}}\left[e^{-im_\phi t}\psi(\boldsymbol{x},t)+e^{im_\phi t}\psi^*(\boldsymbol{x},t)\right]$$

- The dynamics of ψ is given by the standard non-relativistic Hamiltonian:

$$H_{nr}=H_{kin}+H_{int}+H_{grav}$$

(Guth, Hertzberg, and Prescod-Weinstein, 2015; Schiappacasse and Hertzberg, 2017)

$$H_{kin}=\frac{1}{2m_\phi}\int d^3x\,\nabla\psi^*\cdot\nabla\psi\,,\qquad H_{int}=\frac{\lambda}{16m_\phi^2}\int d^3x\psi^{*2}\psi^2,$$

$$H_{grav}=-\frac{Gm_\phi^2}{2}\int d^3x\int d^3x'\,\frac{\psi^*(\boldsymbol{x})\psi^*(\boldsymbol{x}')\psi(\boldsymbol{x})\psi(\boldsymbol{x}')}{|\boldsymbol{x}-\boldsymbol{x}'|}$$

- H_{nr} carries a global $\mathrm{U}(1)$ symmetry $\psi\to\psi e^{i\theta}$ associated with a conserved particle number

$$N=\int d^3x\,\psi^*(\boldsymbol{x})\psi(\boldsymbol{x})$$

- From Hamilton equation ➡ Equation of motion of the field in the non-relativistic regime

$$i\dot{\tilde{\psi}} = -\frac{1}{2}\tilde{\nabla}^2\tilde{\psi} + \tilde{\psi}\tilde{\phi}_N - \frac{\tilde{\psi}^*\tilde{\psi}^2}{8},$$

$$\tilde{\nabla}^2\tilde{\phi}_N = 4\pi\left|\tilde{\psi}\right|^2$$

$\tilde{\phi}_N = \tilde{\phi}_N(\tilde{\psi}^*, \tilde{\psi})$
is the dimensionless (non-dynamical) Newtonian potential

- All quantities have been re-scaled for numerical purposes as

$$x = \left(\frac{m_{pl}\gamma^{1/2}}{m_\phi F_a}\right)\tilde{x}, \qquad t = \left(\frac{{m_{pl}}^2\gamma}{m_\phi {F_a}^2}\right)\tilde{t}$$

$$\psi = \left(\frac{{m_\phi}^{1/2}{F_a}^2}{m_{pl}\,\gamma}\right)\tilde{\psi}, \qquad \phi_N = \left(\frac{{F_a}^2}{{m_{pl}}^2\gamma}\right)\tilde{\phi}_N$$

SPHERICALLY SYMMETRIC CLUMP CONDENSATES

$\Psi(r)$ describes the radial profile
μ describes the correction to the frequency

- The true BEC ground state is guaranteed to be spherically symmetric: $\psi(r,t) = \Psi(r)e^{-i\mu t}$

- The time independent field equation for a spherically symmetric eigenstate is

$$V_{nr} = -\gamma \frac{\Psi^4}{16{F_a}^2}$$

$$\mu\Psi = -\frac{1}{2m}\left(\Psi'' + \frac{2}{r}\Psi'\right) - 4\pi G m^2 \Psi \int_0^\infty dr' r'^2 \, \frac{\Psi(r')^2}{r_>} + \frac{1}{2}\frac{\partial V_{nr}}{\partial \Psi}$$

(Schiappacasse and Hertzberg, 2018)

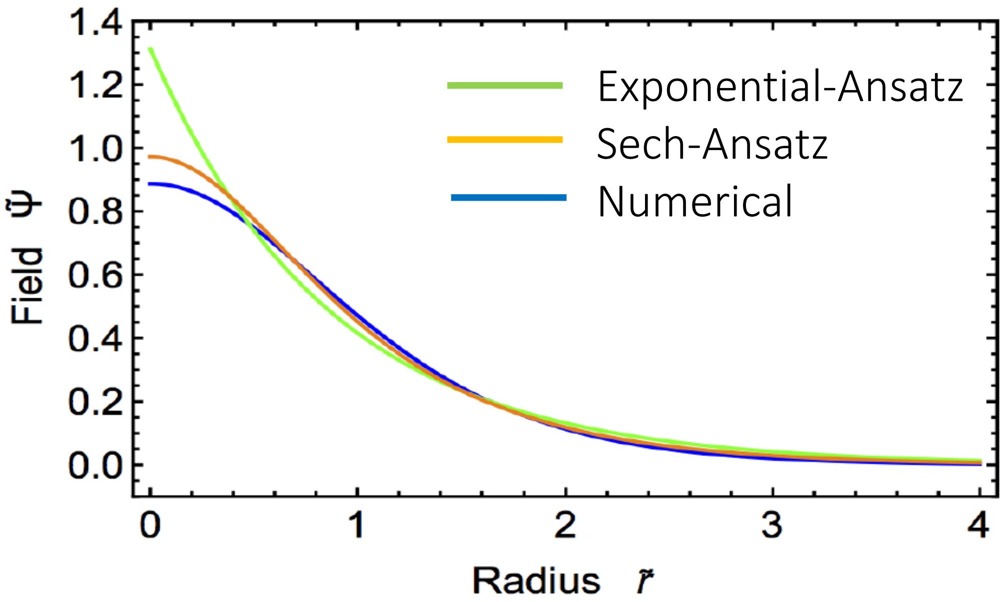

SECH ANSATZ

Length Scale

$$\Psi(r) = \Psi_0 \,\mathrm{sech}(r/R) \quad \text{with } \Psi_0 = \sqrt{\frac{3N_*}{\pi^3 R^3}}$$

Far field region ($\boldsymbol{r} \to \infty$) : Identical to the structure of the time independent Schrödinger equation for the hydrogen atom under replacement $Gm^2N \to e^2$

Near field region ($\boldsymbol{r} \to \boldsymbol{0}$) : Corrections from self-interactions become important. There are no know full analytic solutions.

Stable Branch for axion clumps

Any localized anstaz of a single parameter R

$$\tilde{H}(\tilde{R}) = a\frac{\tilde{N}_*}{\tilde{R}^2} - b\frac{\tilde{N}_*^{\,2}}{\tilde{R}} + c\frac{\tilde{N}_*^{\,2}}{\tilde{R}^3}$$

- $H = \left(\frac{F_a^3}{m_{pl} m_\phi \gamma^{3/2}}\right)\tilde{H}$
- $R = \left(\frac{m_{pl}\gamma^{1/2}}{m_\phi F_a}\right)\tilde{R}$
- $N_* = \left(\frac{m_{pl} F_a}{m_\phi^{\,2}\gamma^{1/2}}\right)\tilde{N}_*$
- $M_* = m_\phi N_*$

$$N_* = 4\pi \int_0^\infty |\psi(r,t)|^2\, r^2 dr$$

R is the effective radius of the solution (variational parameter)

- Apply $\frac{d\tilde{H}}{d\tilde{R}} = 0$ to obtain conditions for stationary solutions
- For any value of $(\tilde{a}, \tilde{b}, \tilde{c})$ there ate two branches of solutions

$$\tilde{R} = \frac{a \pm \sqrt{a^2 - 3bc\tilde{N}^2}}{b\tilde{N}}$$

State of minimum energy at fixed N (spherically symmetry)

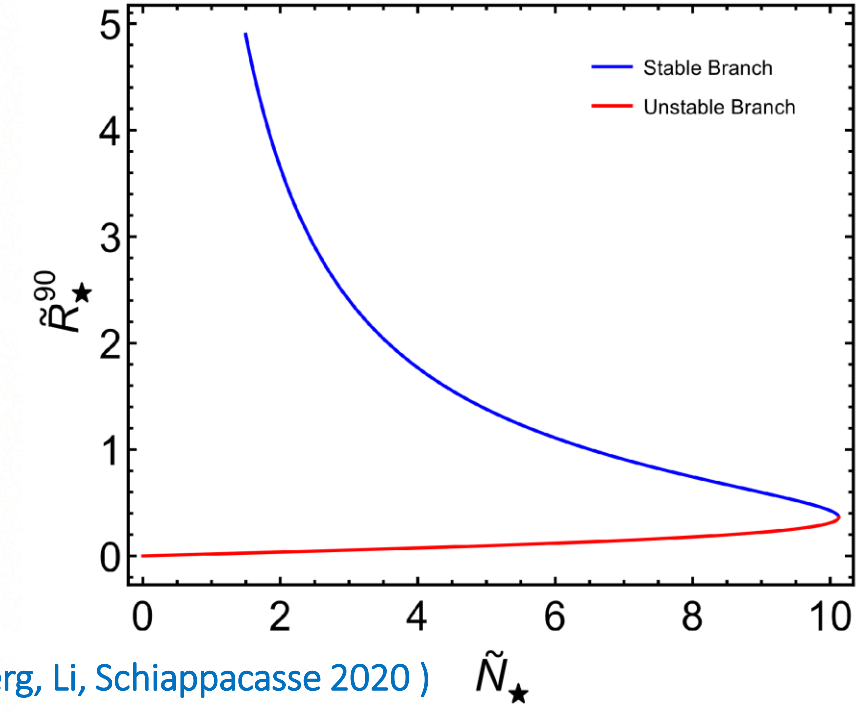

(Hertzberg, Li, Schiappacasse 2020)

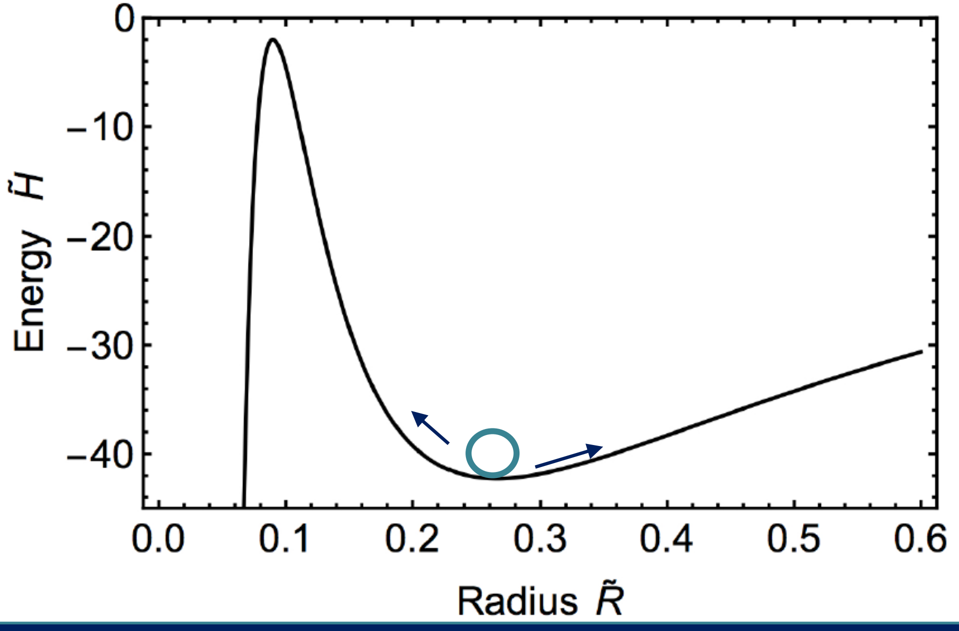

Physical Parameters for Axion Clumps

- We compute the maximum number of particles, the maximum mass, and the minimum clump size for axion clumps as follows:

$$M_{*,max} \sim 2.4 \times 10^{19}\,\mathrm{kg}\left(\frac{10^{-5}\mathrm{eV}}{m_\phi}\right)\left(\frac{F_a}{6\cdot 10^{11}\mathrm{GeV}}\right)\left(\frac{\gamma}{0.3}\right)^{1/2}$$

$$R^{90}_{*,min} \sim 80\ \mathrm{km}\left(\frac{10^{-5}\mathrm{eV}}{m_\phi}\right)\left(\frac{6\cdot 10^{11}\mathrm{GeV}}{F_a}\right)\left(\frac{0.3}{\gamma}\right)^{1/2}$$

- A simple manipulation allows us to express (M_*, R_*) of any clump as

$$M_*(R_*) = \alpha M_{*,max}\left(R^{90}_{*,min}\right)$$

$$R_* = g(\alpha) R^{90}_{*,min} = \left(\frac{1+\sqrt{1-\alpha^2}}{\alpha}\right) R^{90}_{*,min}$$

$$\boldsymbol{\alpha \in [0, 1]}$$

AXIONS AND PHOTONS

- The axion-photon decay channel runs through the chiral anomaly

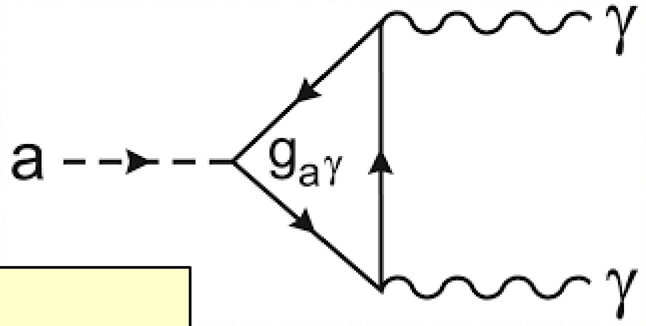

$$L_{EM} = -\frac{1}{4} F_{\mu\nu} F^{\mu\nu} - \frac{g_{a\gamma\gamma}}{4} \phi F_{\mu\nu} \tilde{F}^{\mu\nu}$$

$g_{a\gamma} = \frac{\beta}{F_a}$ } KSVZ/DFSZ/Hidden sector
($\beta \sim 10^{-2}$ in QCD conventional axion models)

Kim (1979); Zhitnitsky (1980)

We send $g_{a\gamma} \to |g_{a\gamma}|$ for ease notation
(Only its magnitude is of significance here)

- Using $\hat{A}^{\mu} = (\hat{A}_0, \hat{\boldsymbol{A}})$ in the Coulomb Gauge, we obtain for the 2 degrees of freedom :

$$\ddot{\hat{\boldsymbol{A}}} - \nabla^2 \hat{\boldsymbol{A}} + g_{a\gamma} \nabla \times \left[(\partial_t \phi) \hat{\boldsymbol{A}} \right] = 0 \longrightarrow \ddot{\hat{\boldsymbol{A}}}_{\boldsymbol{k}} + k^2 \hat{\boldsymbol{A}}_{\boldsymbol{k}} + g_{a\gamma} i\boldsymbol{k} \times \int \frac{d^3k'}{(2\pi)^3} \partial_t \phi_{\boldsymbol{k}-\boldsymbol{k}'} \hat{\boldsymbol{A}}_{\boldsymbol{k}'} = 0$$

$|\nabla \phi| \ll |\partial_t \phi|$ in the non-relativistic limit for axions

- Here $\mu_H^* \approx g_{a\gamma} m_\phi \phi_0/4$ is the maximum growth for the homogeneous case
- Here $\mu_{esc} \approx \frac{1}{2R_*}$

- Numerical solutions show that the growth rate from a localized (spherically) clump is well approximated by :

$$\mu^* \approx \begin{cases} \mu_H^* - \mu_{esc}, & \mu_H^* > \mu_{esc} \\ 0, & \mu_H^* < \mu_{esc} \end{cases}$$

- Taking the sech ansatz profile to set the axion field amplitude, the Resonance Condition reads :

$$g_{\phi\gamma\gamma} F_a > 0.28 \left(\frac{\gamma}{0.3}\right)^{1/2} \left[\frac{g(\alpha)}{\alpha}\right]^{1/2}$$

- In conventional QCD axion models, $g_{a\gamma} = \frac{O(10^{-2})}{f_a}$.

  The resonance could be possible only in unconventional axions models or for couplings to hidden sector photons .

(Daido, Takahashi and N. Yokozaki 2018)

(Hertzberg, Li, Schiappacasse 2020)

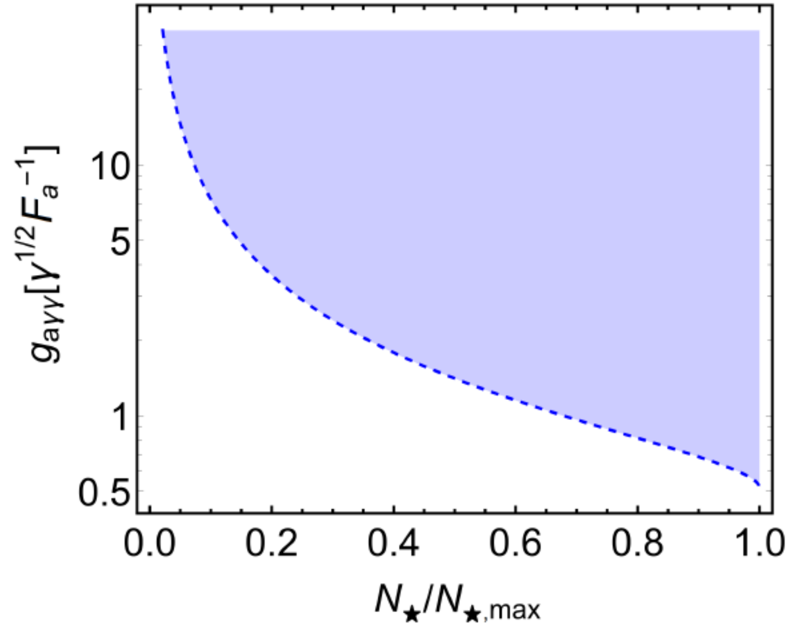

Parameter space for the axion-photon coupling $g_{a\gamma\gamma}[\gamma^{1/2}F_a^{-1}]$ with respect to the number of particles on the stable blue branch, normalized to $N_{\star,\max}\,[m_{\rm Pl}F_a m_\phi^{-2}\gamma^{-1/2}]$. Parametric resonance of axion clumps into photons occurs in the upper right blue shaded region.

AXION STAR MERGER

- We perform a full 3-dimensional simulations of pairs of axion clumps.

- We determine conditions under which merges take place through the emission of scalar waves

  - Head-on collisions
  - Non-head-on Collisions
  - Phase dependence
  - Relative velocities

- We solve the Schrodinger equation by using a symmetric split-step beam method in a tri-dimensional grid with the addition of a spherical sponge

$$\tilde{\psi}(\tilde{\boldsymbol{x}},\tilde{t}+\Delta\tilde{t}) = e^{-i\int_{\tilde{t}}^{\tilde{t}+\Delta\tilde{t}}\tilde{H}d\tilde{t}'}\tilde{\psi}(\tilde{x},\tilde{t}) \approx e^{-i\tilde{V}\frac{\Delta\tilde{t}}{2}}e^{i\frac{\tilde{\nabla}^2}{2}\Delta\tilde{t}}e^{-i\tilde{V}\frac{\Delta\tilde{t}}{2}}\tilde{\psi}(\tilde{x},\tilde{t})$$

$$\tilde{V}(\tilde{\boldsymbol{x}},\tilde{t}) = \tilde{\phi}_N\left(\tilde{\psi}(\tilde{\boldsymbol{x}},\tilde{t})\right) - \frac{|\tilde{\psi}|^2(\tilde{\boldsymbol{x}},\tilde{t})}{8}$$

Head-on Collisions

(Hertzberg, Li, Schiappacasse 2020)

$$\tilde{\psi}(\tilde{\mathbf{x}})_{\text{initial}} = \tilde{\psi}(\sqrt{\tilde{x}^2 + \tilde{y}^2 + (\tilde{z} + \tilde{z}_0)^2})e^{i\tilde{v}_{\tilde{z}}\tilde{z}} + \tilde{\psi}(\sqrt{\tilde{x}^2 + \tilde{y}^2 + (\tilde{z} - \tilde{z}_0)^2})e^{-i\tilde{v}_{\tilde{z}}\tilde{z}}$$

with $\tilde{v}_{\tilde{z}} = (m_{\rm Pl}\gamma^{1/2}/F_a)\, v_z$

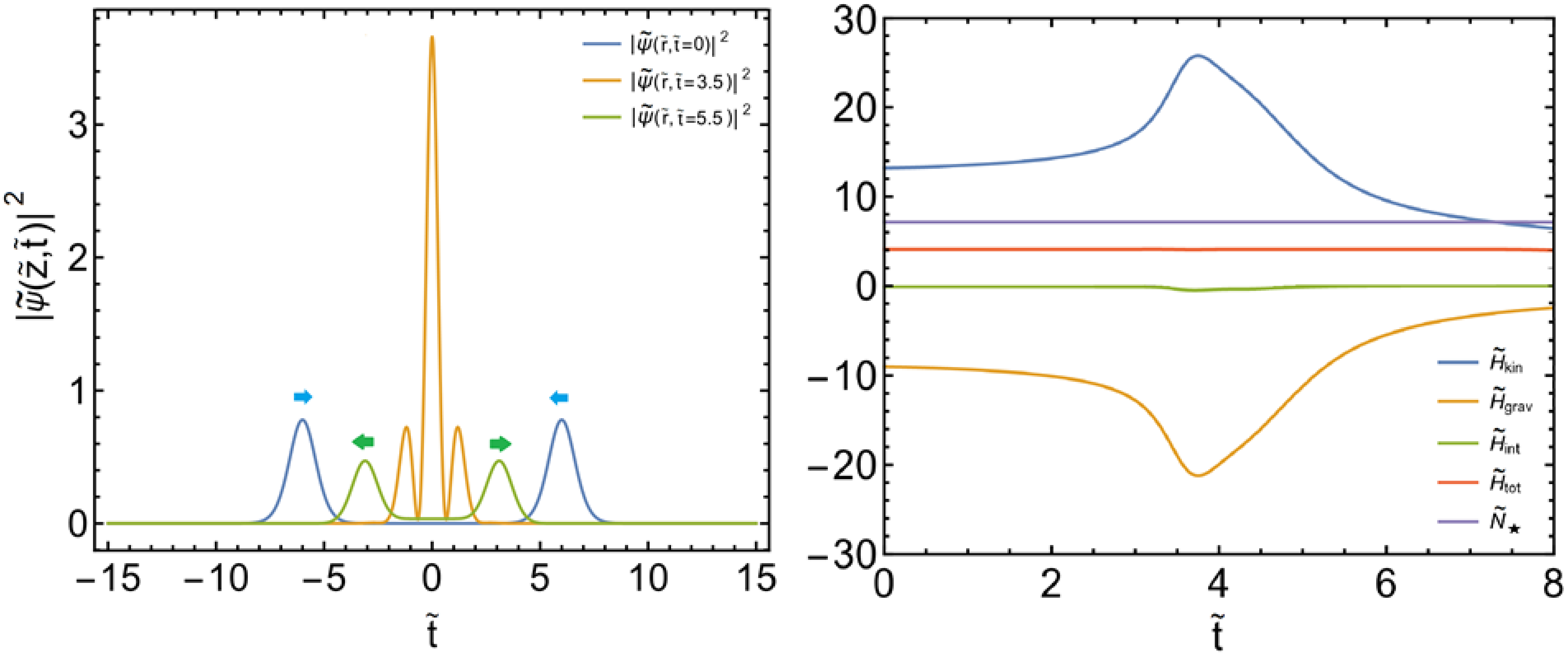

Head-on collision of two clumps each with $\tilde{N}_\star = 3.5650$. Here $\tilde{v}_{\tilde{z}} = 1.5$ in (Left) Dimensionless local number density along the $\tilde{z}$-direction with $(\tilde{x}, \tilde{y}) \simeq (0, 0)$ at times: $\tilde{t} = 0$, $\tilde{t} = 3.5$, and $\tilde{t} = 5.5$. (Right) Time evolution of the dimensionless total energy (and their components) from the collision of the two clumps. The traveling clumps pass through each other without merging.

The initial total energy of the system is positive

Unbounded System

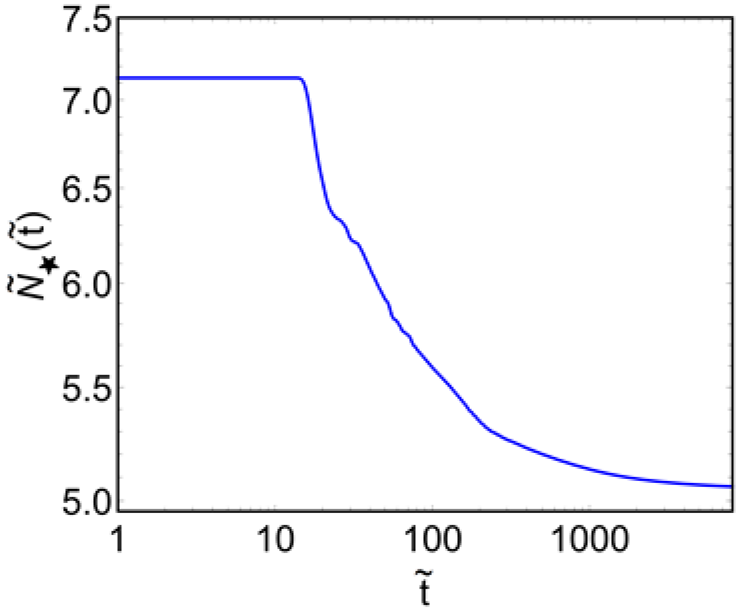

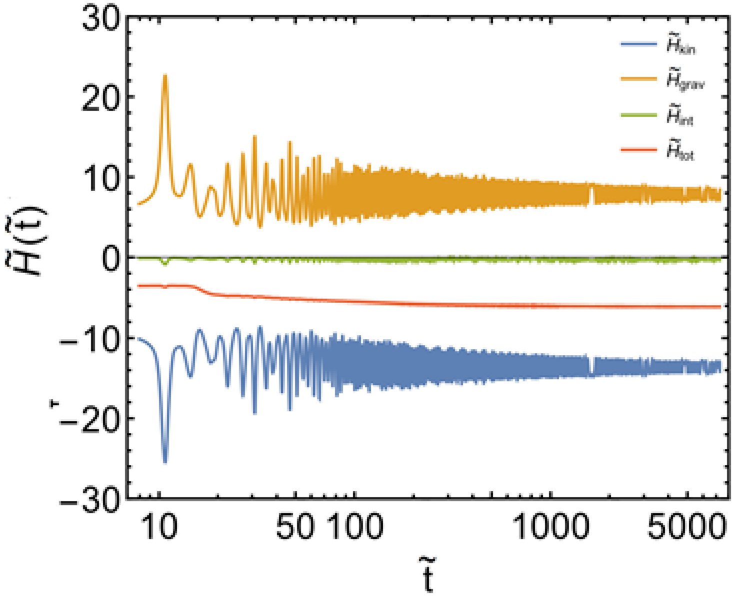

: Head-on collision of two clumps each of one with $\tilde{N}_\star = 3.56503$. Here $\tilde{v}_{\tilde{z}} = 0.3$ and $\tilde{z}_0 = 6$ We have used a cosmological box with a volume $(384)^3$ in dimensionless units and a temporal and spatial sizes equal to $\Delta\tilde{t} = 0.082$ and $(\Delta\tilde{x}, \Delta\tilde{y}, \Delta\tilde{z}) \simeq 0.078$, respectively. (Left) Evolution of the dimensionless number of particles of the system during the whole simulation. (Right) Evolution of the total energy of the system and their different components ($\tilde{H}_{\rm kin}$, $\tilde{H}_{\rm grav}$, and $\tilde{H}_{\rm int}$). The reduction in total number and total energy over time is due to emission of scalar waves that go into absorbing boundary conditions.

$$t \sim 2\ \text{yrs} \left(\frac{\gamma}{0.3}\right)\left(\frac{10^{-5}\text{eV}}{m_\phi}\right)\left(\frac{6\cdot 10^{11}\text{GeV}}{F_a}\right)^2$$

$$\tilde{N}^*_{\rm final} \simeq 0.7\left(\tilde{N}_{*,1} + \tilde{N}_{*,2}\right)$$

$$\text{with} \quad \tilde{N}_{*,1} = \tilde{N}_{*,2} = 3.56503$$

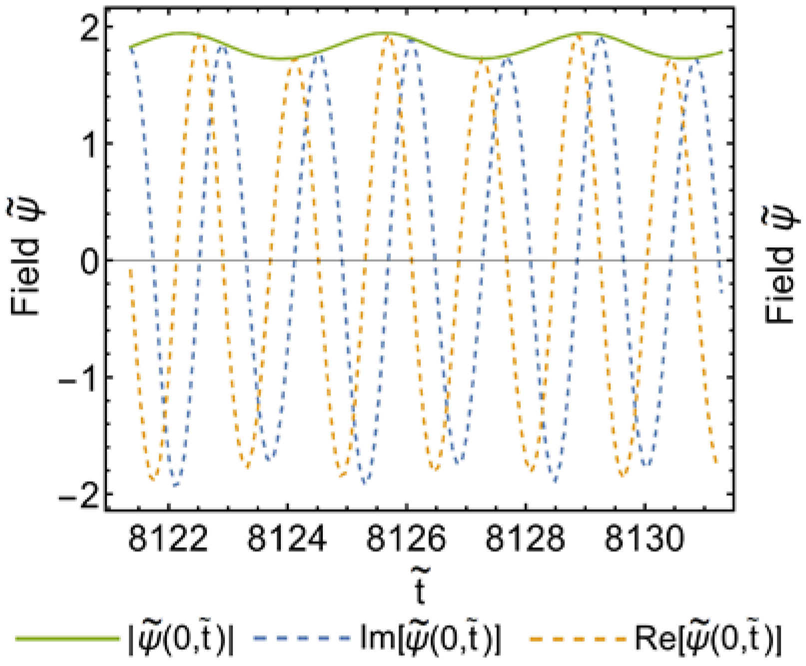

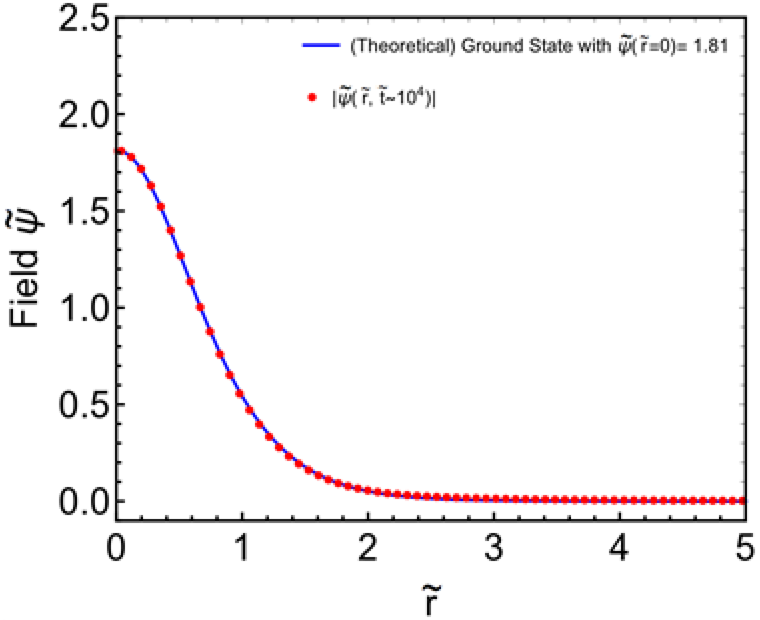

(Left) Value of the field at late times after the merger of two (stable) ground state clumps as detailed in Fig. 6. (Left) The field value at the origin $(\tilde{x}, \tilde{y}, \tilde{z}) = (0, 0, 0)$; green solid curve is absolute value of field, dashed blue curve is imaginary part of field, and dashed orange curve is real part of field. (Right) Red points are absolute value of the field in the $\tilde{z}$-direction with $(\tilde{x}, \tilde{y}) = (0, 0)$ of the resultant clump at $\tilde{t} = 8121$. Blue solid curve is theoretical (stable) ground state configuration with $\tilde{\Psi}(\tilde{r} = 0) = 1.814$

	$\tilde{H}_{\rm kin}$	$\tilde{H}_{\rm grav}$	$\tilde{H}_{\rm int}$	$\tilde{H}_{\rm total}$
Stable Ground State ($\tilde{\Psi}(\tilde{r} = 0) = 1.814$)	7.5356	-14.1402	-0.3103	-6.9149
$\lvert\tilde{\psi}(\tilde{r}, \tilde{t} \simeq 8 \times 10^3)\rvert$	7.4980	-13.8390	-0.3085	-6.6495
Porcentual Relative Error (ξ)	0.5%	2.1%	0.6%	3.8%

The initial total energy of the system is negative → Bounded System

Parameter Space for Merger

- If $H_{Total}^{Initial} > 0$ clumps will merge after collision leading to a resultant clump

- If the initial separation of clumps is large enough, we may estimate the total initial energy as

Gravitational attraction between clumps

$$\boldsymbol{H_{Total}^{Initial} = (H_{kin,1} + H_{grav,1} + H_{int,1}) + (H_{kin,2} + H_{grav,2} + H_{int,2}) + H_1^{cm} + H_2^{cm} + H_{grav}^{*-*}}$$

Kinetic energy of the center of mass of each clump

- Using the sech ansatz approximation and going to the dimensionless variables,

$$\tilde{H} \simeq \frac{2ab^2\tilde{N}_*^3}{\left(a + \sqrt{a^2 - 3bc\tilde{N}_*^2}\right)^2} - \frac{2b^2\tilde{N}_*^3}{a + \sqrt{a^2 - 3bc\tilde{N}_*^2}} - \frac{2b^3c\tilde{N}_*^5}{\left(a + \sqrt{a^2 - 3bc\tilde{N}_*^2}\right)^3} + \tilde{N}_*\tilde{v}_{\tilde{z}}^2 - \frac{\tilde{N}_*^2}{2\tilde{z}_0}$$

$$v_z = \left(\frac{F_a}{m_{pl}\gamma^{1/2}}\right)\tilde{v}_{\tilde{z}}$$

Since clumps today in galactic halos have relative velocities $\sim 10^2$ km, we need for a typical pair of clumps to merge $F_a \gtrsim 10^{15}\mathrm{GeV}$

For $F_a \ll 10^{15}\mathrm{GeV}$, there is still possibility of merger since the clump relative velocity has a zero mean

(Left) Initial total (dimensionless) energy of the system, $\tilde{H}_{\mathrm{total}}$, with respect to the magnitude of the maximum initial velocity of both two clumps, $\tilde{v}_{\tilde{z},\max}$, to lead to a merger after a head-on collision. A sech ansatz is used to approximate the clumps radial profile. Results are shown for different initial total number of particles. In particular, green, orange, red and blue line refer to the cases $\tilde{N}_{\star,1} = \tilde{N}_{\star,2} = (3, 5, 6, 0.7\tilde{N}_{\star,\max})$, respectively. The initial distance between the center of mass of the clumps is set to be $2 \times 8R$, where R is the clump lenght scale . (Right) Contour-level of the clumps critical relative velocity $v_{\mathrm{rel,\ crit}}$ [km/s] in the parameter space $(\tilde{N}_{\star,1} = \tilde{N}_{\star,2}, F_a)$, e.g. the initial number of particles of each clump and the PQ symmetry breaking scale, respectively. The critical relative velocity for clumps is calculated using $\tilde{v}_{\tilde{z},\mathrm{crit}} = \tilde{v}_{\tilde{z},\mathrm{crit}}(\tilde{N}_{\star,1} = \tilde{N}_{\star,2})$ from the plot on the left

(Hertzberg, Li, Schiappacasse 2020)

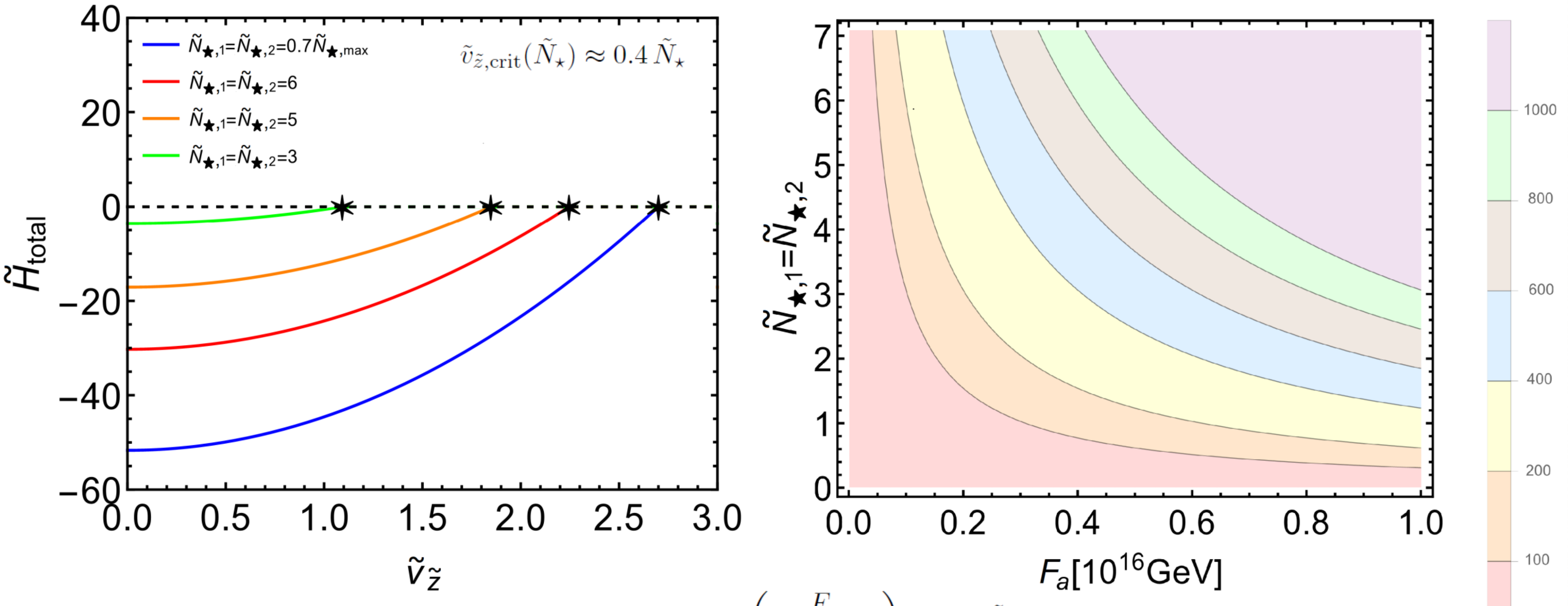

$$v_{\mathrm{rel,\ crit}} \simeq 2 \times 448\,\mathrm{km/s}\left(\frac{F_a}{10^{16}\,\mathrm{GeV}}\right)\tilde{v}_{\tilde{z},\mathrm{crit}}(\tilde{N}_\star)$$

Collision and Meger Rate

- The collision rate per halo per year between axion stars with $(M_{*,1}, M_{*,2}) \simeq M_*$ in the galactic halo:

$$\Gamma_{*-*} = 4\pi \int_0^{R_{200}} \frac{r^2}{2} \left(\frac{\rho(r)_{halo} f_*^{\mathrm{DM}}}{M_*} \right)^2 \langle \sigma_{eff}(v_{rel}) v_{rel} \rangle dr$$

$$\sigma_{eff}(v_{rel}) = 4\pi R_*^2 \left(1 + \frac{2 G_N M_*}{R_* v_{rel}^2} \right)$$

$$\langle \sigma_{eff}(v_{rel}) v_{rel} \rangle \sim 4\pi \int_0^{v_{esc}} p_0 \; e^{-v^2/v_0^2} \sigma_{eff}(v) v^3 dv$$

- A first estimate comes from a homogeneous Galactic halo, e.g. $M_{200} \sim 10^{12} M_\odot$ and $\bar{\rho}_{halo} \sim 200 \rho_m^0$ such that $M_{200} = (4\pi/3) \bar{\rho}_{halo} R_{200}^3$

Here p_0 is obtained from the normalization of the Gaussian velocity probability distribution in the Galactic frame as $4\pi \int_0^{v_{esc}} v^2 p(v) dv = 1$

$$\Gamma_{*-*}^{hom} \sim 3 \left[\frac{(g(\alpha)/\alpha)|_{\alpha=0.5}}{7.46} \right]^2 \left(\frac{f_*^{DM}}{0.01} \right)^2 \left(\frac{\gamma}{0.3} \right)^2 \left(\frac{6 \cdot 10^{11} \mathrm{GeV}}{F_a} \right)^4 \left[1 + 10^{-7} \left[\frac{7.46}{(g(\alpha)/\alpha)|_{\alpha=0.5}} \right] \left(\frac{F_a}{6 \cdot 10^{11} \mathrm{GeV}} \right)^2 \left(\frac{0.3}{\gamma} \right) \right] \frac{collision}{year \cdot galaxy}$$

Becomes significant at $F_a \gtrsim 10^{15} \mathrm{GeV}$

(Left) Collision rate for close encounters between axion dark matter clumps versus the PQ scale using a homogeneous density for the Milky Way halo (blue line) and three different mass profile for the halo. We have used for all cases $N_{\star,1} = N_{\star,2} = 0.4N_{\rm max}$ and $f_\star^{\rm DM} = 0.01$. We have used halo parameters (best-fit models) obtained in Refs. [111] (NFW profile), [112] (Burkert profile), and [112] (NFW profile) in red, purple, and orange lines, respectively. The purple line corresponds to the homogeneous case at which $\bar\rho_{\rm halo} \sim 200\rho_m^0$. (Right) Collision rate for close encounters between axion dark matter clumps versus the PQ scale for the parameter space $(0.005, 10^{-4}) \leq (\alpha, f_\star^{\rm DM}) \leq (0.7, 10^{-1})$ (orange shaded region), where $N_{\star,1} = N_{\star,2} = \alpha N_{\rm max}$. In particular, blue, red and orange lines correspond to values $(\alpha, f_\star^{\rm DM}) = (0.7, 10^{-4}), (0.4, 10^{-2}), (0.005, 10^{-1})$, respectively. The collision rate for all cases is calculated by using a NFW profile for the dark matter halo [111].

Table 2: Main dark matter halo parameters for three different Milky Way mass models (best-fit models).

Profile	R_{200} [kpc]	M_{200} [$M_\odot$]	r_s [kpc]	ρ_s [GeV/cm^3]	$\rho_\odot$ [GeV/cm^3]	$R_\odot$ [kpc]	v_0 [km/s]	$v_{\rm esc}$ [km/s]
NFW [111]	237	1.43×10^{12}	20.2	0.32	0.395	8.29	239	622
B [112]	291	1.11×10^{12}	9.26	1.57	0.487	7.94	241	576
NFW [112]	319	1.53×10^{12}	16.1	0.53	0.471	8.08	244	613

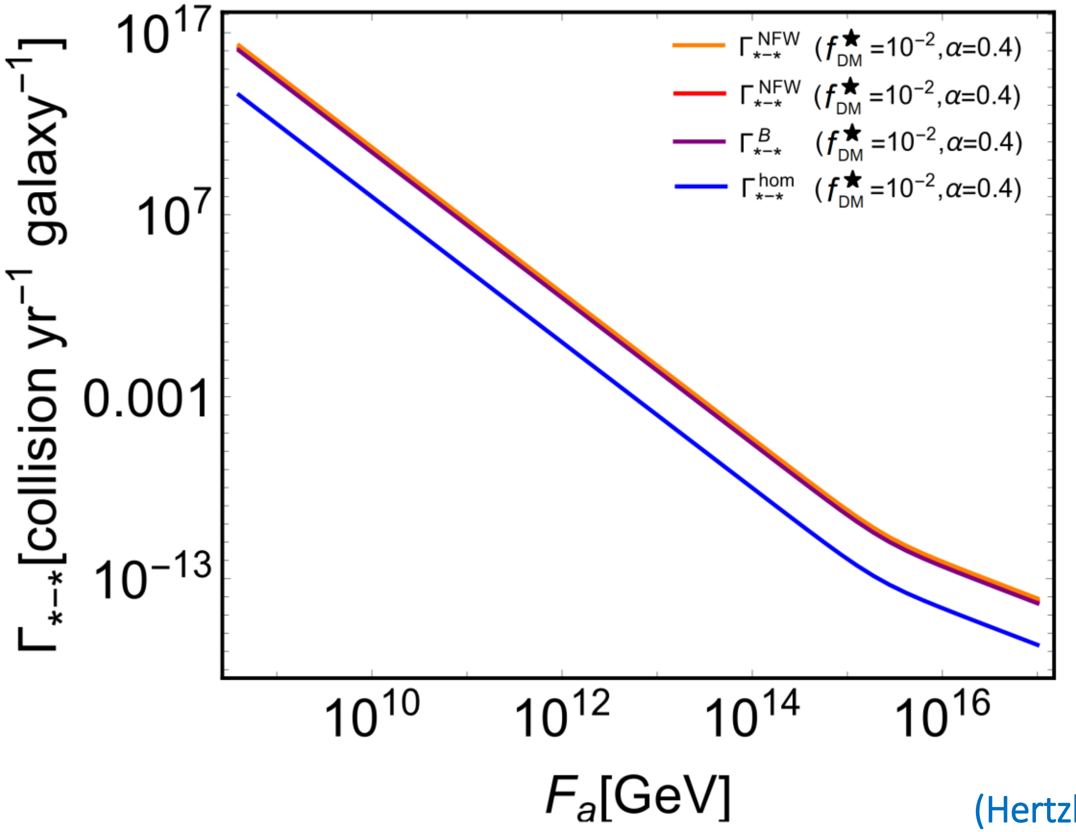

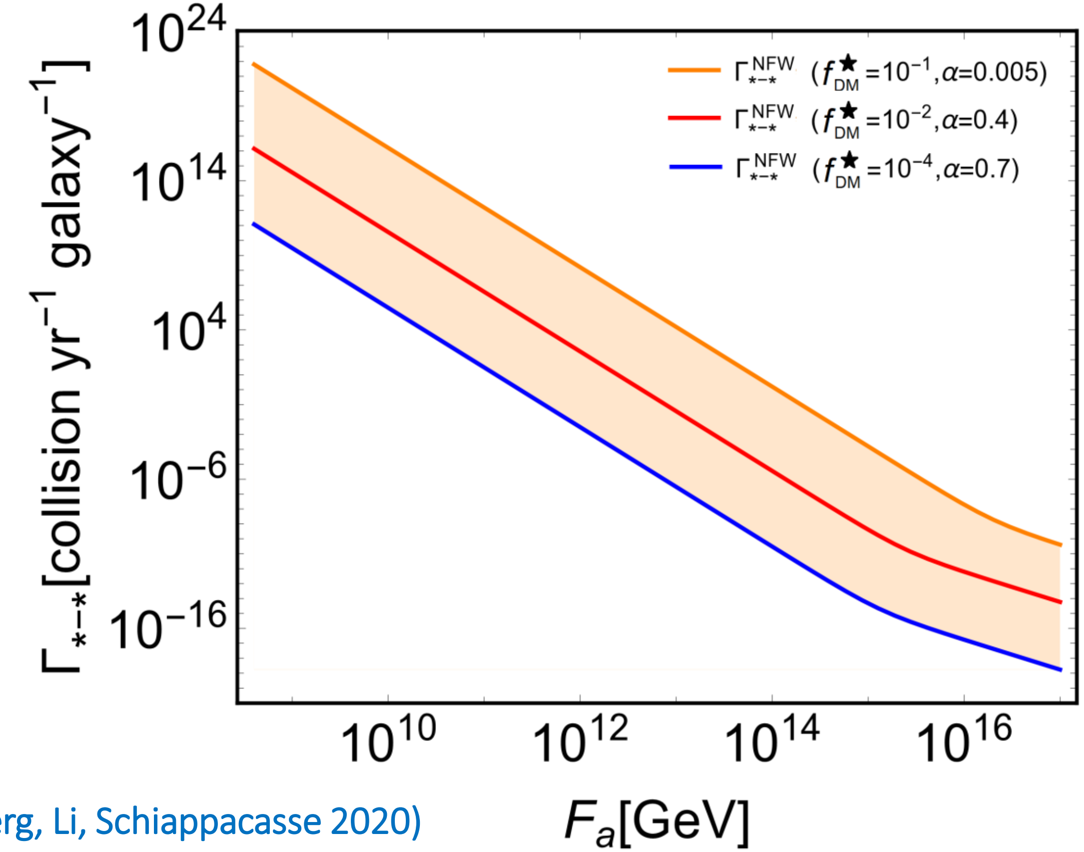

(Hertzberg, Li, Schiappacasse 2020)

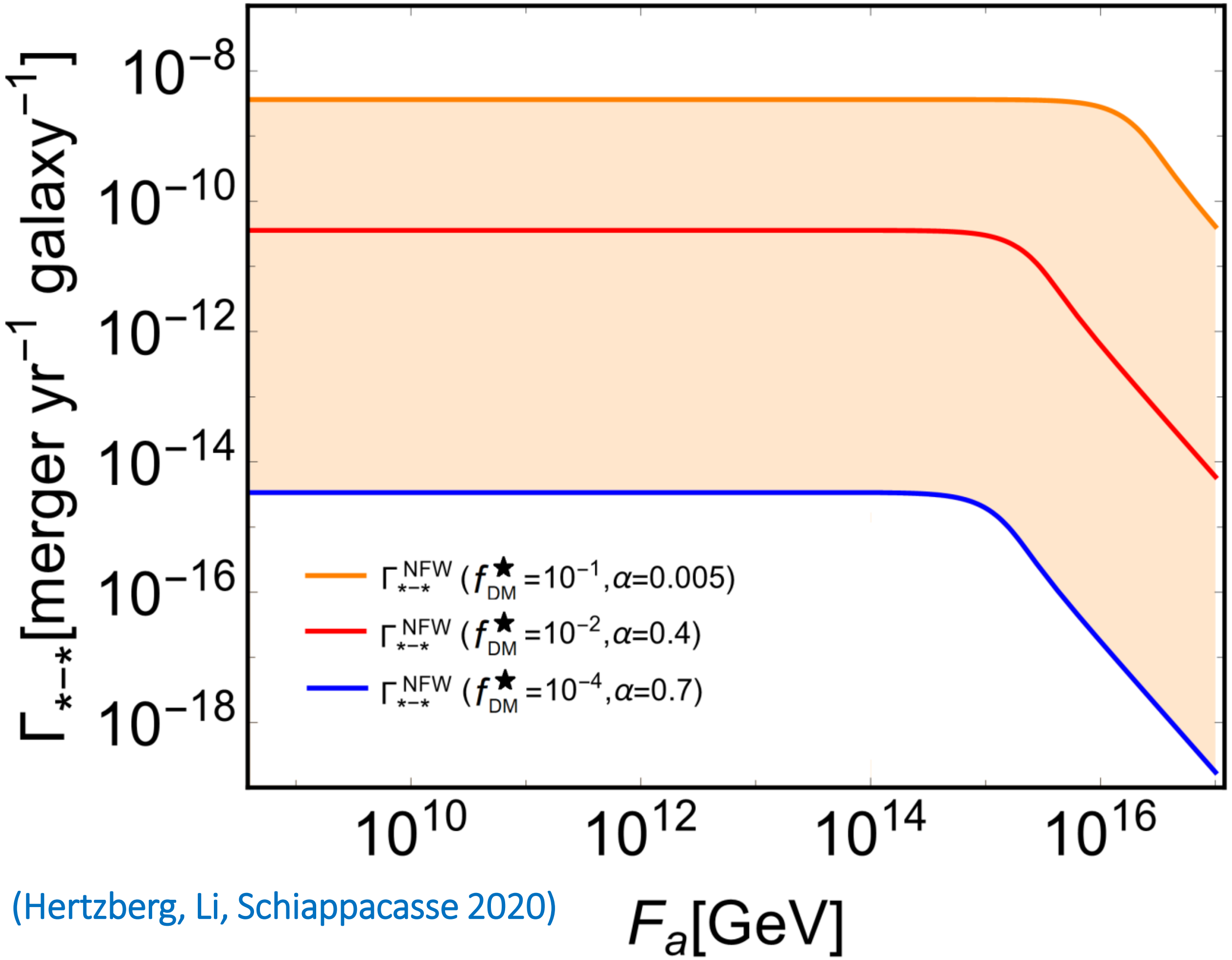

(Hertzberg, Li, Schiappacasse 2020)

Merger rate from pair-wise interactions from a single collision between axion dark matter clumps versus the PQ scale to the decay constant for the parameter space $(0.005, 10^{-4}) \leq (\alpha, f_\star^{\rm DM}) \leq (0.7, 10^{-1})$ (orange shaded region), where $N_{\star,1} = N_{\star,2} = \alpha N_{\rm max}$. As in Fig. 11, the blue, red and orange lines correspond to values $(\alpha, f_\star^{\rm DM}) = (0.7, 10^{-4}), (0.4, 10^{-2}), (0.005, 10^{-1})$, respectively. The collision rate for all cases is calculated by using a NFW profile for the dark matter halo [111], and making the simplified assumption that mergers arise from 2-body pair-wise interactions only. For small F_a this provides a conservative lower bound on the actual merger rate, which can be enhanced due to 3-body processes, etc.

Typical speeds for stars in the galaxy indicate that they typically carry too much energy for a 2-body merger to take place when PQ scale is small.

We replace v_{esc} by $v_{rel,crit}$ as the upper limit of the integral which leads to $\langle \sigma_{eff}(v_{rel}) v_{rel} \rangle$

- Merger rate from pair-wise interactions from a single collision between axion dark matter clumps
- This is a conservative lower bound, since 3-body interactions and multiple encounters can enhance it.

Photon Emission

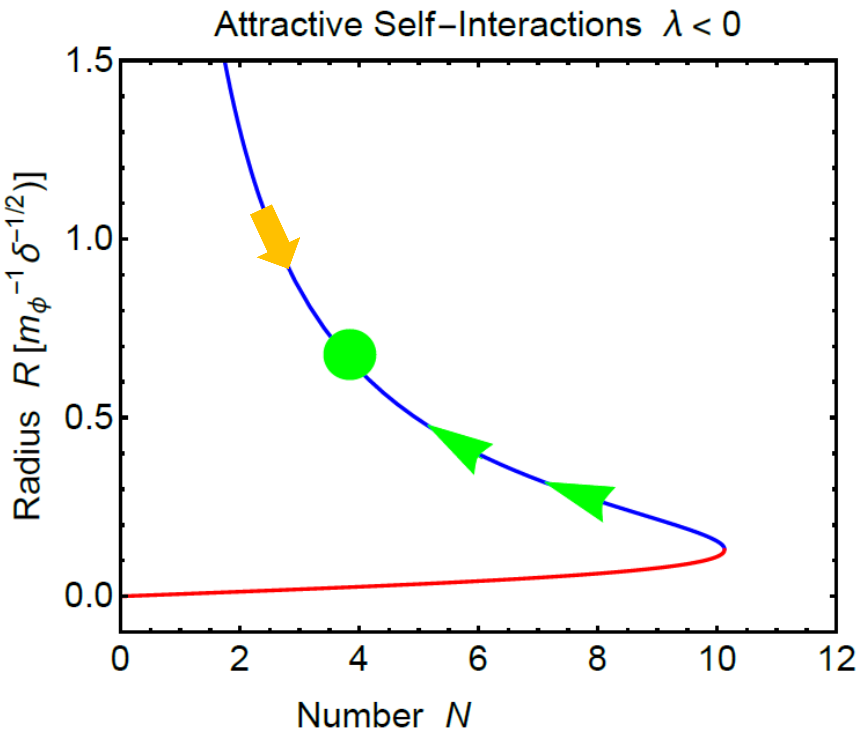

- Suppose $g^*_{a\gamma\gamma} > g_{a\gamma,min}$. All clumps having $N_* > N^*_c$ they will undergo to parametric resonance into photons : $N_* \to N^*_c$.

- All clumps with $N_* < N^*_c$ will tend to capture axion dark matter from the background and to move down through the blue curve so that $N_* \to N^*_c$.

- Kind of PILE-UP at a unique value of number of particles or mass for axion dark matter clumps in the galactic halo today.

- After axion star formation in the earlier history of the universe, we expect a distribution for number of particles as shown in the blue curve.

Under suitable conditions, we found that clumps can merge and produce a new clump according to the relation

$$N^*_{final} \sim 0.7(N_{*,1} + N_{*,2}) \simeq 1.4 N_*$$

Since $N_* \gtrsim N^*_c$, the new clump will undergo parametric resonance as soon as it settles down to a ground state configuration.

- The energy released by the electromagnetic radiation during resonance,

$$E_{*,\gamma} = \left[0.7\left(\widetilde{N}_{*,1} + \widetilde{N}_{*,2}\right) - \widetilde{N}_c^*\right] \frac{m_{pl} F_a}{m_\phi \gamma^{1/2}} \simeq 1.4(\alpha - 0.71\alpha_c) M_{*,max}$$

where $N_* = \alpha N_{*,max}$, $N_c^* = \alpha_c N_{*,max}$ and $M_{*,max} \sim 1.4 \cdot 10^{46}\mathrm{GeV} \left(\frac{10^{-5}\mathrm{eV}}{m_\phi}\right)\left(\frac{F_a}{6 \cdot 10^{11}\mathrm{GeV}}\right)\left(\frac{0.3}{\gamma}\right)^{1/2}$

- The time scale for the exponential growth can be estimated from the growth rate, $\tau \approx \frac{1}{\mu_H^*} = \frac{g_{a\gamma} m_\phi \phi_0}{4}$:

$$\tau \lesssim 2 \cdot 10^{-4}\mathrm{s}\; g(\alpha) \left(\frac{\gamma}{0.3}\right)^{1/2} \left(\frac{6 \cdot 10^{11}\mathrm{GeV}}{F_a}\right)\left(\frac{10^{-5}\mathrm{eV}}{m_\phi}\right)$$

The electromagnetic radiation output corresponds to a narrow line near the resonant wavelength

$$\lambda_{EM} \approx \frac{4\pi}{m_\phi}$$

The bandwidth can be estimated from the width of the first instability band for the homogeneous case, $\Delta k \approx g_{a\gamma\gamma} m_\phi \phi_0 / 2$

$$\nu_{EM} \approx 1.2\ \mathrm{GHz} \left(\frac{m_\phi}{10^{-5} eV}\right) \pm \frac{1.6\mathrm{kHz}}{g(\alpha)} \left(\frac{F_a}{6 \cdot 10^{11} GeV}\right)\left(\frac{m_\phi}{10^{-5}\mathrm{eV}}\right)\left(\frac{0.3}{\gamma}\right)^{1/2}$$

Detectability

- For the QCD axion and $10^{10}\mathrm{GeV} \lesssim \mathrm{F_a} \lesssim 10^{13}\mathrm{GeV}$, the central frequency of emisión ranges as $70\mathrm{MHz} \lesssim \nu_{\mathrm{EM}} \lesssim 70\ \mathrm{GHz}$

Collisions between isolated pair of axion clumps which typically lead to merger require large values of the axion decay constant.

Mergers for moderate values of $\mathrm{F_a}$ are still viable since the collision rate is much more larger in that regime

1) Arecibo Observatory (300 MHz – 10 GHz)
2) Five Hundred meter Aperture radio Telescope (70 MHz – 3 GHz)
3) Karl G. Jansky Very Large Array (1 GHz – 50 GHz)
4) Green Bank Telescope (290 MHz – 115.2 GHz)
5) The Square Kilometer Array (Phase 1, 50 MHz – 14 GHz)

(Giovanelli et al. 2005, Nan et al. 2011)

- For $\mathrm{F_a} \gtrsim 10^{15}\ \mathrm{GeV}$, mergers of axion clumps are more robust, but the resonant axion decay leads to low frequency photon emission which would require radio telescopes from space to be detected.

The Orbiting Low Frequency Antennas for Radio Astronomy Mission (OLFAR) is an ambitious plan of building a swarm of hundreds to thousands of satellites to analyze frequencies below 30 MHz

(Bentum et al 2020)

- The received flux per bandwidth (spectral flux density) is quite appreciable, since the signal is highly monochromatic:

$$S_B = \frac{\Delta E/\Delta t}{4\pi\, D^2 \Delta\nu_{EM}} \sim 3\cdot 10^{-6} W/m^2/Hz(\alpha - 0.71\alpha_c)\left(\frac{F_a}{6\cdot 10^{11}\mathrm{GeV}}\right)\left(\frac{10^{-5}\mathrm{eV}}{m_\phi}\right)\left(\frac{50\; kpc}{D}\right)^2\left(\frac{0.3}{\gamma}\right)^{1/2}$$

- The smallest spectral flux density that a radio telescope can detect depends on the observation time (t_{obs}), signal bandwidth (ΔB), effective collective telescope area (A_{eff}), and system temperature (T_{sys}) as

$$S_{B,min} \approx 9\cdot 10^{-28} W/m\text{^}2/H_z \left(\frac{1\; MH_z}{\Delta B}\right)^{1/2}\left(\frac{1\; ms}{t_{obs}}\right)^{1/2}\left(\frac{10^3 m^2/K}{A_{eff}/T_{sys}}\right)$$

Take SKA (Phase 1): $S_{B,min} \approx 3\cdot 10^{-28} W/m^2/H_z \left(\frac{1\; MH_z}{\Delta B}\right)^{1/2}\left(\frac{1\; ms}{t_{obs}}\right)^{1/2}$

In the frequency range detectable for SKA, we have $S_B \gg S_{B,min}$ for emissions in the Galaxy

DISCUSSION

- We have explored a novel way to possibly detect axion dark matter by computing axion star merger and the posible resulting resonance into photons.

For moderate $g_{\phi\gamma\gamma}$ clumps, there is a critical mass for clumps M_c^* beyond which they can undergo parametric resonance of photons

To have clumps above the critical mass (M_c^*) in the galaxy today would require mergers.

$$M_{\text{final}}^* \simeq 0.7\left(M_{*,1} + M_{*,2}\right)$$

$$\text{with} \quad M_{*,1} \sim M_{*,2}$$

- For smaller F_a, the number of clumps and their cross sections are large so that collisions are very frequent in the galaxy today.

However, such clumps have small binding energy so that such collisions tipically do not lead to mergers

However, this can happen via statistical flukes in the Galaxy due to the Maxwellian distribution of relativities velocities.

- Typical collisions which lead to mergers require $F_a \gtrsim 10^{15}\mathrm{GeV}$, but in this case the rate of collisions is much smaller.

- In many string compactifications, the axion decay constant is in the range $10^{15}\mathrm{GeV} - 10^{18}\mathrm{GeV}$.
- In addition, apart from the presence of QCD axion plausibly embedded in this framework, string models predict the presence of many axion-like particles. (Arvanitaki et al. 2020)

Kinetic nucleation of axion stars in mini-halos around PBHs and axion-like-particles clumps formed by tachionic instability hold for general values of the PQ symmetry scale

(Hertzberg, Schiappacasse, Yanagida 2020) & (Fukunaga et al. 2020)

- Higher decay constant models refer to smaller axion masses so that we will need radiotelescopes with sensitivity to rather low frequencies for resonance detection.
- The relaxation time toward to the ground state (after collision) is quite long so that the resonance may be is a gradual process

Lower flux of photons on the Earth

SOME REFERENCES

- M. P. Hertzberg, Y. Li, E. D. Schiappacasse, "Merger of Dark Matter Clumps and Resonant Photon Emission", arXiv:2005.02405 (2020). Accepted in JCAP.
- E. D. Schiappacasse and M. P. Hertzberg, "Analysis of Dark Matter Axion Clumps with Spherical Symmetry," JCAP **1801**, 037 (2018).
- M. P. Hertzberg and E. D. Schiappacasse, "Scalar Dark Matter Clumps with Angular Momentum," JCAP **1808**, 028 (2018).
- M. P. Hertzberg and E. D. Schiappacasse, "Dark Matter Axion Clump Resonance of Photons," JCAP **1811**, 004 (2018).
- G. Choi, H. He and E. D. Schiappacasse, "Probing Dynamics of Boson Stars by Fast Radio bursts and Gravitational Wave Detection," JCAP **1910**, 043 (2019).
- M. P. Hertzberg, E. D. Schiappacasse and T. T. Yanagida, "Axion Star Nucleation in dark minihalos around Primordial Black Holes," arXiv:2001.07476 [astro-ph.CO] (2020). Accepted in JCAP.
- J. Preskill, M. B. Wise and F. Wilczek, "Cosmology of the Invisible Axion," Phys. Lett. B **120**, 127 (1983).
- R. D. Peccei and H. R. Quinn, "CP Conservation in the Presence of Instantons," Phys. Rev. Lett. **40,** 279 (1978).
- S. Weinberg, "A New Light Boson?," Phys. Rev. Lett. **40**, 223 (1978).
- J. E. Kim, ''Weak Interaction Singlet and Strong CP Invariance,'' Phys. Rev. Lett. **43**, 103 (1979).
- A. R. Zhitnitsky, "On Possible Suppression of the Axion Hadron Interactions. (In Russian)," Sov. J. Nucl. Phys. **31**, 260 (1980).
- A. H. Guth, M. P. Hertzberg and C. Prescod-Weinstein, "Do Dark Matter Axions Form a Condensate with Long-Range Correlation?," Phys. Rev. D **92**, 103513 (2015).
- G. Grilli di Cortana, E. Hardy, J. Pardo Vega and G. Villadoro, "The QCD axion, precisely," JHEP **1601**, 034 (2016).
- N. W. McLachlan, *Theory and Application of Mathieu Functions* (Oxford University Press, London, 1947), Chap. 6.
- R. Daido, F. Takahashi and N. Yokozaki, "Enhanced axionphoton coupling in GUT with hidden photon," Phys. Lett. B **780**, 538 (2018).
- M. P. Hertzberg, "Quantum Radiation of Oscillons," Phys. Rev. D **82**, 045022 (2010).
- M. Kawasaki and M. Yamada, "Decay rates of Gaussian-type I-balls and Bose-enhancement effects in 3+1 dimensions," JCAP 1402, 001 (2014).

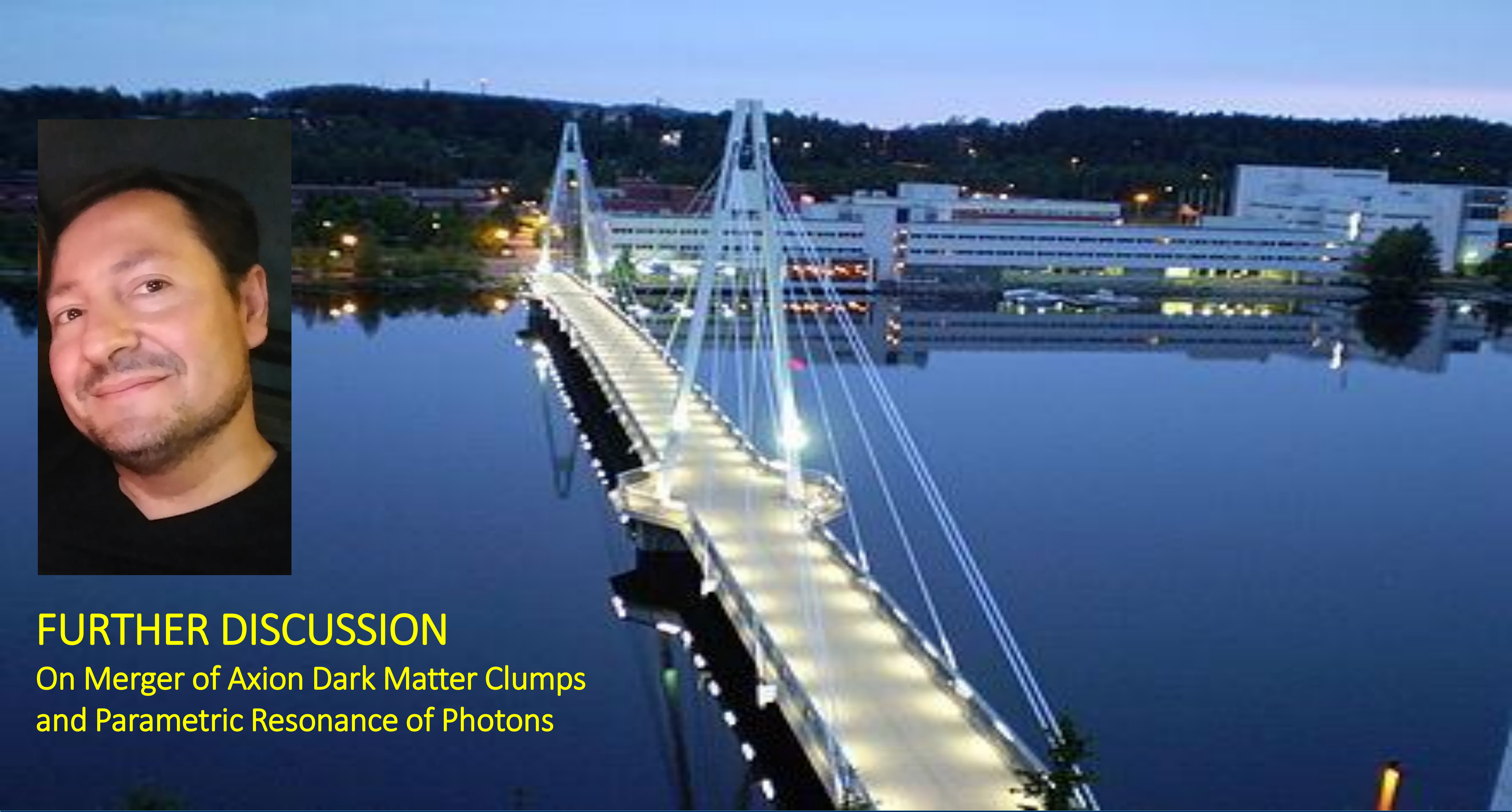

FURTHER DISCUSSION

On Merger of Axion Dark Matter Clumps and Parametric Resonance of Photons

AXION STAR NUCEATION IN DARK HALOS AROUND PBHs

(Hertzberg, Schiappacasse, Yanagida 2020).

- Codark matter scenario:

AXIONS (mass m_a) + PBHs

Dark minihalo formation around PBHs with radius R_{halo} and mass M_{halo}

$$M_{\rm halo}(z) = 3\left(\frac{1000}{1+z}\right) M_{\rm PBH}\,,$$

$$R_{\rm halo}(z) = 0.019\,{\rm pc}\left(\frac{M_{\rm halo}}{M_\odot}\right)^{1/3}\left(\frac{1000}{1+z}\right).$$

Condensation time scale

- Axion stars may kinetically nucleate in mini-halos before time of first Galaxy formation

$$\tau_{\rm gr} \simeq \frac{4\sqrt{2}}{27\pi}\left(\frac{R_{\rm halo}}{v_a}\right)(R_{\rm halo} m_a v_a)^3$$

$$(m_a v_a)\times(R_{\rm halo}) \gg 1\,,$$

$$(m_a v_a^2)\times(\tau_{\rm gr}) \gg 1\,.$$

v_a Virial velocity of axion in minihalos

Condition for Kinetic nucleation

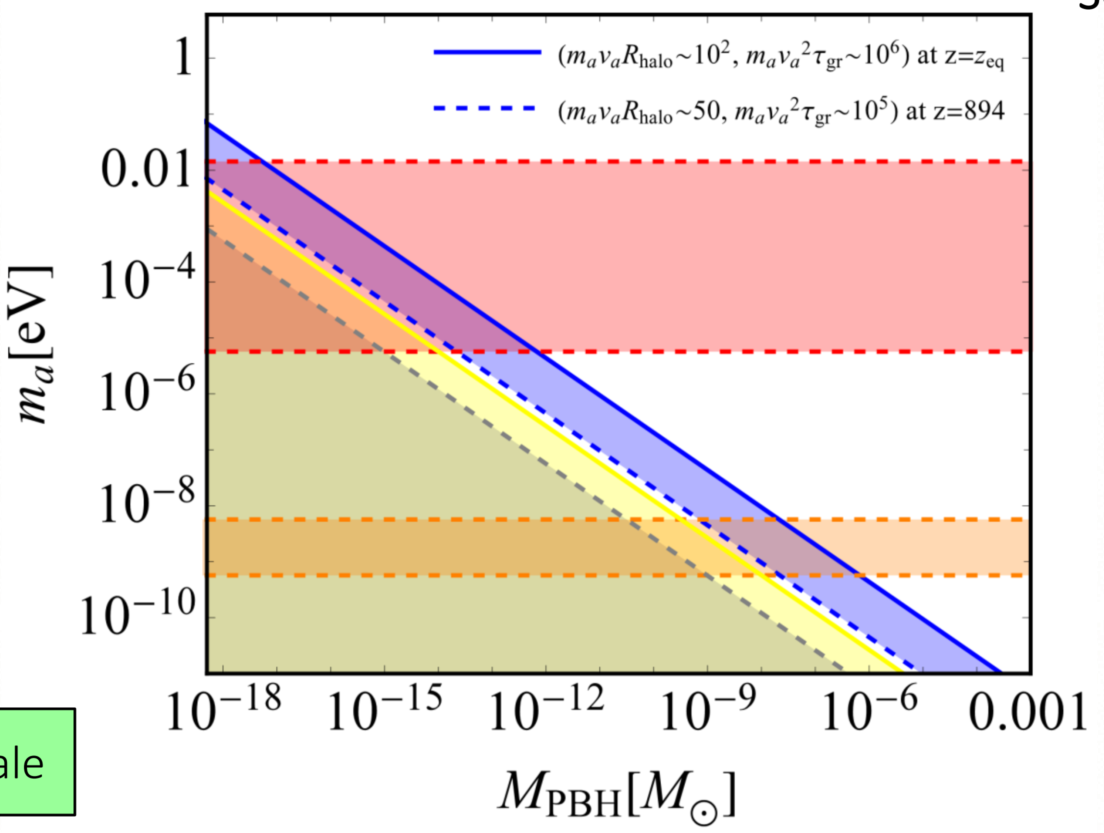

Contour-levels of $(m_a v_a R_{\rm halo}, m_a v_a^2 \tau_{\rm gr})$ at a given redshift z in the parameter space $(M_{\rm PBH}, m_a)$. The blue shaded region between the blue solid ($z = z_{\rm eq}$) and dashed ($z = 894$) lines corresponds to the parameter space of $(M_{\rm PBH}, m_a)$ at $894 < z < z_{\rm eq}$, which satisfies the kinetic regime as $(m_a v_a R_{\rm halo}, m_a v^2 \tau_{\rm gr}) \gtrsim (50, 10^5)$. The intersection between the red (orange) band and the blue shaded region corresponds to the parameter space for the QCD (string) axion, where $4\times 10^8\,{\rm GeV} \gtrsim F_a \gtrsim 10^{12}\,{\rm GeV}$ (where $10^{15}\,{\rm GeV} \gtrsim F_a \gtrsim 10^{16}\,{\rm GeV}$ [43, 44]). The yellow solid (gray dashed) line plus the yellow (gray) shaded region correspond to the zone in which $\lambda_{\rm DB}/R_{\rm halo} \geq 1$ at $z_{\rm eq}$ (at $z = 894$)

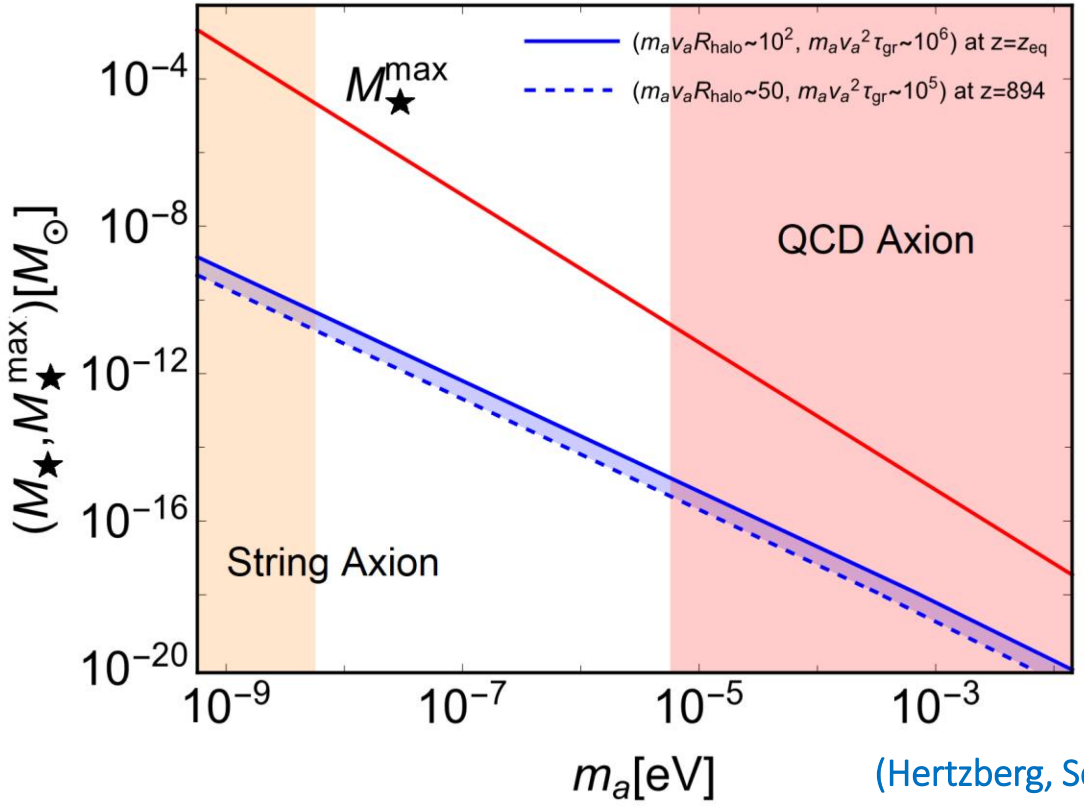

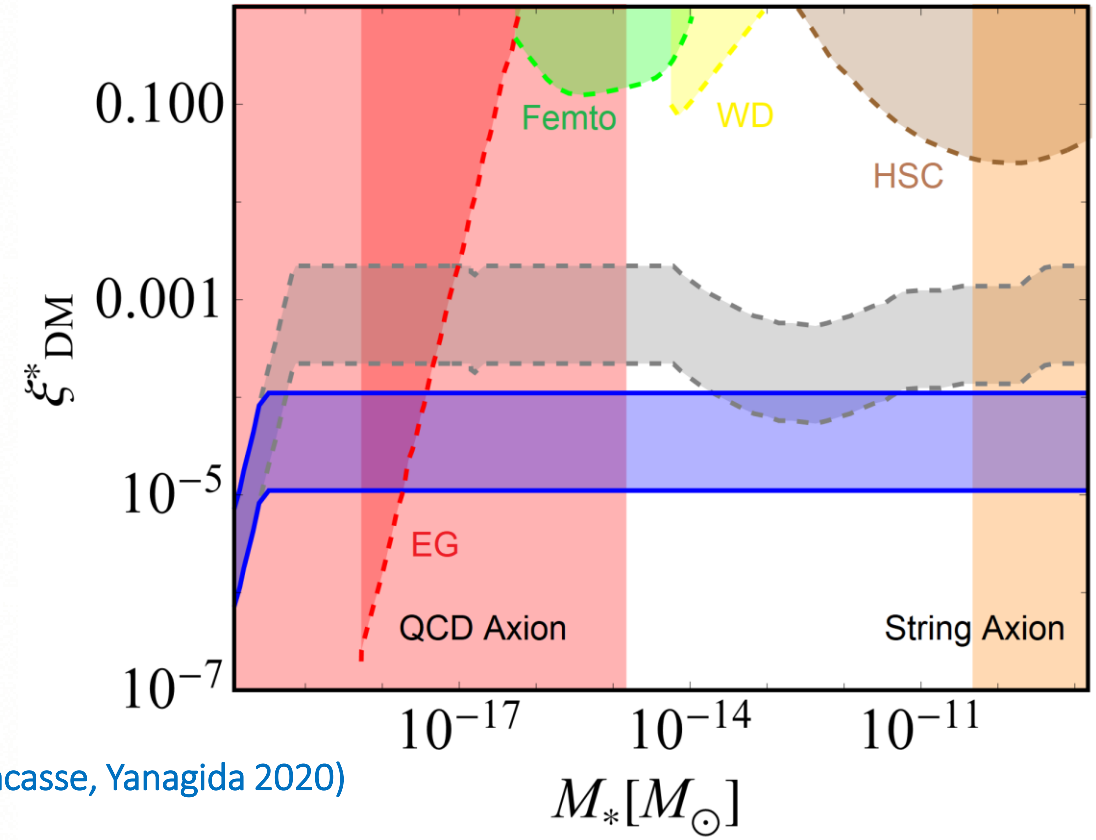

(Hertzberg, Schiappacasse, Yanagida 2020)

Contour-levels of $(m_a v_a R_{\rm halo}, m_a v_a^2 \tau_{\rm gr})$ in the parameter space $(m_a, M_\star)$. The blue shaded region between the blue solid $(z = z_{\rm eq})$ and dashed $(z = 894)$ lines corresponds to the parameter space of $(m_a, M_\star)$ at which the kinetic regime is satisfied as $(m_a v_a R_{\rm halo}, m_a v^2 \tau_{\rm gr}) \gtrsim (50, 10^5)$ at $894 < z < z_{\rm eq}$. Red (orange) band corresponds to the mass range for the QCD (string) axion. The red solid line indicates the theoretical maximum mass, $M_\star^{\rm max}$, that an axion star in the ground state configuration can achieve

The blue (gray) shaded band shows the estimate of the current fraction of dark matter in axion stars $\xi^\star_{\rm DM}$, a fraction in PBHs no greater than 0.5% (10%), $1 \le N_\star \le 10$, and the contour-level $(m_a v_a R_{\rm halo}, m_a v_a^2 \tau_{\rm gr}) \sim (10^2, 10^6)$ at $z = z_{\rm eq}$ in the parameter space $(M_{\rm PBH}, M_\star)$. Light red (light brown) band corresponds to the mass range of axion stars associated with the QCD (string) axion. In additon, we have shown constraints over the PBH abundance. In particular, extragalactic photon background (EG) femtolensing (Femto) , white dwarfs in our local galaxy (WD) and Subaru HSC data (HSC)

EFFECTIVE PHOTON MASS

- In the not-quite-empty space of the interstellar medium, photons acquire an effective mass equal to the plasma frequency as

$$\omega_p^2 = \frac{4\pi\alpha n_e}{m_e} = \frac{n_e}{0.03\text{cm}^{-3}}(6.4\times 10^{-12}\text{eV})^2$$

- Considering the spatial distribution of n_e and the fact that axion clump condensates are moving in the galactic halo: $\omega_p(t) \approx \omega_p f(t)$, where $f(t)$ is a non-periodic time dependent function of orden 1.
- The modified equation for the mode function of the vector potential for the homogeneous case is

$$\ddot{\boldsymbol{s}}_k + [k^2 + \omega_p^2(t) - g_{a\gamma}\omega_0 k\phi_0 \sin(\omega_0 t)]s_{\boldsymbol{k}} = 0$$

- Taking $k \approx (m_\phi/2)$ and using as reference the amplitude ϕ_0 evaluated for the case of a sech ansatz, we have

$$\frac{\omega_p^2}{(g_{a\gamma}\omega_0 k\phi_0)} \sim \frac{10^{-23}}{\left(\frac{\beta}{10^{-2}}\right)10^{-19}} \sim 10^{-4}$$

So, we expect that the effect of the effective photon mass in the resonance should be negligible

- We begin by treating the axion field as homogeneous since this case is the simplest possible

The axion field is treat as a classical oscillatory background:
$\phi(t) = \phi_0 \cos(\omega_0 t)$, where $\omega_0 \approx m_\phi$

In general such configuration is unstable to collapse from gravity and attractive self-interactions:
Homogeneous Condensate → Clump Condensate

(Guth, Hertzberg, and Prescod-Weinstein, 2015)

- Clearly, the equation of motion for $\widehat{\boldsymbol{A}}_{\boldsymbol{k}}$ decouple in k-space. Then, expressing $\widehat{\boldsymbol{A}}_{\boldsymbol{k}}$ in function of vectors for circular polarizations and modes functions $s_{\boldsymbol{k}}(t)$ we have

$$\ddot{\widehat{\boldsymbol{A}}}_{\boldsymbol{k}} + k^2 \widehat{\boldsymbol{A}}_{\boldsymbol{k}} - g_{a\gamma}\omega_0\phi_0 i\boldsymbol{k} \times \widehat{\boldsymbol{A}}_{\boldsymbol{k}} = 0 \quad \longrightarrow \quad \ddot{s}_{\boldsymbol{k}} + \underbrace{[k^2 - g_{a\gamma}\omega_0\phi_0 \sin(\omega_0 t)]}_{\omega_k^2(t)} s_{\boldsymbol{k}} = 0$$

$$\omega_k^2(t) = \omega_k^2(t + 2\pi/\omega_0)$$

- In the parameter space of Mathieu equation (ME) there is a band structure of unstable (resonant) and stable regions:

(McLachlan, 1947)

$$s_{\mathbf{k}}(t) = P_{\mathbf{k}}(t)e^{\mu_{\mathbf{k}}t} + P_{\mathbf{k}}(-t)e^{-\mu_{\mathbf{k}}t}$$

GENERAL SOLUTION

If the Floquet exponent, μ_{k} , has a real part, the resonance occurs

- At small amplitude of weak coupling limit of $(k/\omega_0) \gg (g_{a\gamma}\phi_0/2)$, we have a spectrum of narrow resonant bands equally spaced at $(k/\omega_0)^2 \approx (n/2)^2$ for n a positive integer.

- Expand the solution for each circularized polarization as:

$$s_{\mathbf{k}}(t) = \sum_{\omega} e^{i\omega t} f_{\omega}(t)$$

Slowing varying

The band width and Floquet exponent magnitude decreases as n increases

Plug into ME and focus on lowest frequencies $(\omega = \pm\omega_0/2)$

$$\frac{d}{dt}\begin{bmatrix} f_{\omega_0/2} \\ f_{-\omega_0/2} \end{bmatrix} = \frac{i}{\omega_0}\begin{bmatrix} A - \frac{\omega_0^2}{4} & -i\frac{B}{2} \\ -i\frac{B}{2} & -A + \frac{\omega_0^2}{4} \end{bmatrix}\begin{bmatrix} f_{\omega_0/2} \\ f_{-\omega_0/2} \end{bmatrix}$$

Positive eigenvalues previous matrix

- The growth rate is: $\mu_k = \sqrt{\frac{g_{a\gamma}^2 k^2 \phi_0^2}{4} - \frac{\left(k^2 - \frac{\omega_0^2}{4}\right)^2}{\omega_0^2}}$
- For $\Re(\mu_k) > 0$: Exponentially growing solutions

  (First instability band)
- For $\Re(\mu_k) = 0$: Instability band edges

$$k_{l/r_{edge}} = \sqrt{\frac{\omega_0^4}{4} + \frac{g_{a\gamma}^2 \omega_0^2 \phi_0^2}{16}} \mp \frac{g_{a\gamma}\omega_0\phi_0}{4}$$

$$\boxed{k^* = (\omega_0/2)\sqrt{1 + g_{a\gamma}^2 \phi_0^2/2} \approx m_\phi/2}$$

Center of the band

Maximum Floquet Exponent

$$\boxed{\mu_H^* \approx \frac{g_{a\gamma} m_\phi \phi_0}{4}}$$

Numerical Analysis

(Standard Floquet Method)

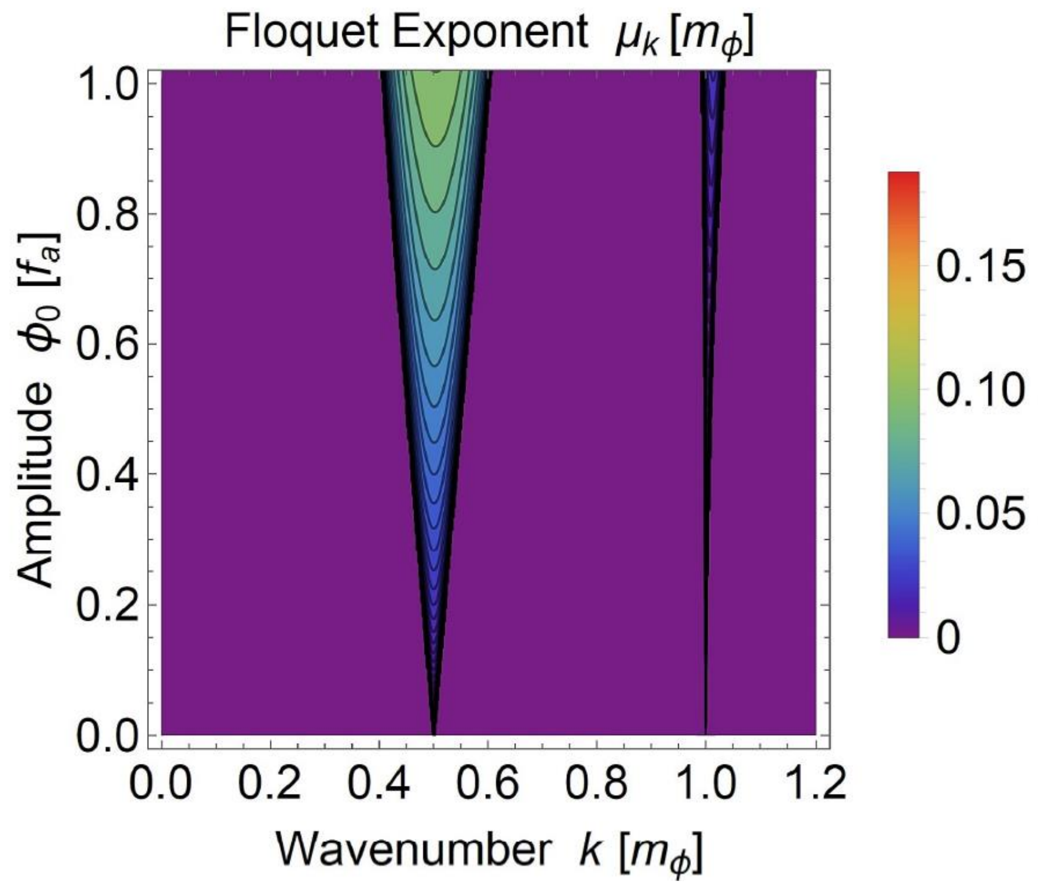

Contour plot of the real part of Floquet exponent μ_k, describing parametric resonance of photons from a homogeneous condensate, as a function of wavenumber k and physical amplitude ϕ_0. We plot ϕ_0 in units of f_a and k & μ_k in units of m_ϕ. We have set $g_{a\gamma} = 0.4/f_a$ to illustrate the behavior, although in conventional QCD axions $g_{a\gamma} = \mathcal{O}(10^{-2})/f_a$ which would give narrower resonance bands.

(Hertzberg and Schiappacasse, 2018)

Vector Spherical Decomposition

- Since $\phi = \phi(r,t)$, the usual 3-dimensional Fourier transform of the equation of motion for the vector potential is not the best way to proceed.
- We prefer performing a vector spherical harmonic decomposition of $\hat{\boldsymbol{A}}$:

$$\hat{\boldsymbol{A}}(\boldsymbol{x},t) = \int \frac{d^3k}{(2\pi)^3} \sum_{lm} \left[\hat{a}(k) v_{lm}(k,t) \boldsymbol{M}_{lm}(k,\boldsymbol{x}) - \hat{b}(k) w_{lm}(k,t) \boldsymbol{N}_{lm}(k,\boldsymbol{x}) \right]$$

- Again neglecting gradients of the axion field,

Here $\boldsymbol{M}_{lm}$, $\boldsymbol{N}_{lm}$ are vector spherical harmonics, where $\boldsymbol{M}_{lm} = \frac{i j_l(kr)}{\sqrt{l(l+1)}} \left[\frac{im}{\sin\theta} Y_{lm} \hat{\theta} - \frac{\partial Y_{lm}}{\partial\theta} \hat{\varphi} \right]$ and

$\nabla \times \boldsymbol{M}_{lm} = -ik\boldsymbol{N}_{lm}$, $\nabla \times \boldsymbol{N}_{lm} = ik\boldsymbol{M}_{lm}$

$$\ddot{\hat{\boldsymbol{A}}} - \nabla^2 \hat{\boldsymbol{A}} + g_{a\gamma} \nabla \times \left[(\partial_t \phi) \hat{\boldsymbol{A}} \right] = 0$$

$$\Downarrow$$

$$\int \frac{d^3k}{(2\pi)^3} \sum_{lm} \left[\left(\ddot{v}_{lm} + k^2 v_{lm} - ik g_{a\gamma} \partial_t \phi w_{lm} \right) \boldsymbol{M}_{lm}(k,\boldsymbol{x}) - \left(\ddot{w}_{lm} + k^2 w_{lm} + ik g_{a\gamma} \partial_t \phi v_{lm} \right) \boldsymbol{N}_{lm}(k,\boldsymbol{x}) \right] = 0$$

It can be solved numerically, but for any arbitrary sum over *{l,m}* is quite complicated

- We choose one resonant channel for simplicity.
- Taking axion field configurations which slowly vary in space and rewriting the axion spatial profile by a 1-dimensional (real) Fourier transform

The system becomes simpler to treat numerically

Channel l=1,m=0

$$w_{10}(k,t) = \pm i v_{10}(k,t)$$

$$\ddot{w}_{10}(k,t) + k^2 w_{10}(k,t) - i g_{a\gamma}\omega_0 k \sin(\omega_0 t) \int \frac{dk'}{2\pi} v_{10}(k',t)\widetilde{\Phi}_{1d}(k-k')=0$$

(1) We compute the resonance structure numerically using Floquet Theory
(2) We use various choices of $g_{a\gamma}$ and parameters of axion clump ($\tilde{R}$ and and $\widetilde{N}_*$)
(3) We operate in the sech approximation on the stable branch:

$\phi(r,t) = \Phi(r)\cos(\omega_0 t) = \sqrt{\frac{2}{m_\phi}}\Psi(r)\cos(\omega_0 t)$ with $\omega_0 = m_\phi + \mu \approx m_\phi$

- Here $\mu_H^* \approx g_{a\gamma} m_\phi \phi_0/4$ is the maximum growth for the homogeneous case
- Here $\mu_{esc} \approx \frac{1}{2R_*}$

- Numerical solutions show that the growth rate from a localized (spherically) clump is well approximated by :

$$\mu^* \approx \begin{cases} \mu_H^* - \mu_{esc}, & \mu_H^* > \mu_{esc} \\ 0, & \mu_H^* < \mu_{esc} \end{cases}$$

- Taking the sech ansatz profile to set the axion field amplitude, the Resonance Condition reads :

$$g_{\phi\gamma\gamma} F_a > 0.28 \left(\frac{\gamma}{0.3}\right)^{1/2} \left[\frac{g(\alpha)}{\alpha}\right]^{1/2}$$

- In conventional QCD axion models, $g_{a\gamma} = \frac{O(10^{-2})}{f_a}$.

  The resonance could be possible only in unconventional axions models or for couplings to hidden sector photons .

(Daido, Takahashi and N. Yokozaki 2018)

(Hertzberg, Li, Schiappacasse 2020)

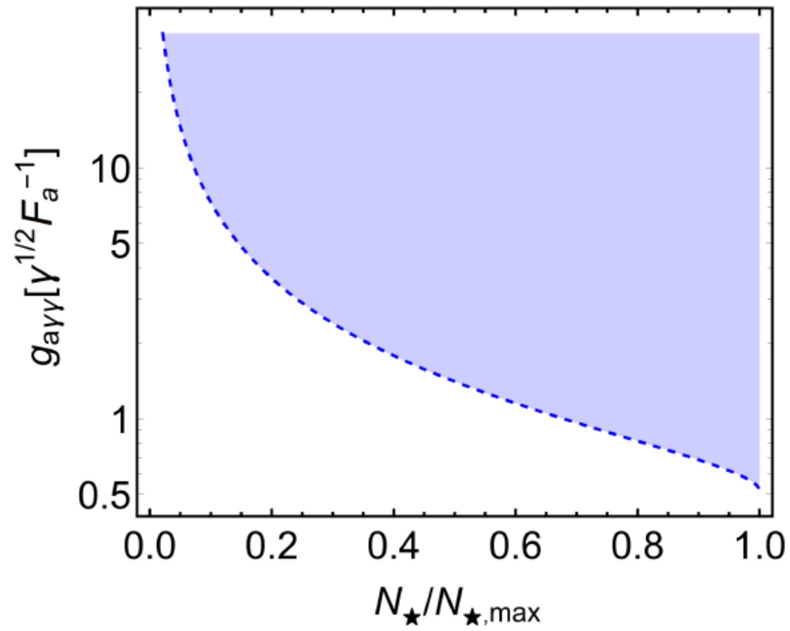

Parameter space for the axion-photon coupling $g_{a\gamma\gamma}[\gamma^{1/2}F_a^{-1}]$ with respect to the number of particles on the stable blue branch, normalized to $N_{\star,\max}\,[m_{\rm Pl}F_a m_\phi^{-2}\,\gamma^{-1/2}]$. Parametric resonance of axion clumps into photons occurs in the upper right blue shaded region.

CLUMP CONDENSATES WITH ANGULAR MOMENTUM

- Clump condensates with non-zero angular momentum have a larger $N_{*,max}$ (and field amplitude).

The angular momentum is $\mathbf{L} = (0,0,N\mathrm{m})$ with $N = 4\pi \int_0^\infty dr\, r^2 |\Psi(r)^2|$

- We take the field profile to be $\psi(x,t) = \sqrt{4\pi}\Psi(r) Y_{\mathrm{lm}}(\theta,\varphi) e^{-i\mu t}$
- We look for states which minimize the energy at fixed particle number and fixed angular momentum
- As usual we make an ansatz for the radial profile $\Psi(r)$: For non-zero l, the structure for small r behavior drastically changes in comparison to the l=0 case

$$\mu_{eff}\Psi \approx -\frac{1}{2m_\phi}\left(\Psi'' + \frac{2}{r}\Psi'\right) + \frac{\mathrm{l}(\mathrm{l}+1)}{2m_\phi r^2}\Psi \quad \text{(near region)}$$

It includes the gravitational term

These terms blow up when $r \longrightarrow 0$

We need $\Psi(r) = \Psi_\alpha r^{\mathrm{l}} - \frac{1}{2}\Psi_\beta r^{\mathrm{l}+2} + \cdots$ (near region)

MODIFIED GAUSSIAN ANSATZ

$$\Psi(r) = \sqrt{\frac{N}{2\pi\left(\mathrm{l}+\frac{1}{2}\right)! R^3}} \left(\frac{r}{R}\right)^{\mathrm{l}} e^{-r^2/(2R^2)}$$

$$\mathrm{H}(R) = a_{\mathrm{lm}}\frac{N}{m_\phi R^2} - b_{\mathrm{lm}}\frac{G m_\phi^2 N^2}{R} + c_{\mathrm{lm}}\frac{\lambda N^2}{m_\phi^2 R^3}$$

The Hamiltonian is a generalization of the previous one for the $l = 0$ case: constant coefficients (a,b,c) become $\{\mathrm{l},\mathrm{m}\}$-dependent

Field $\tilde{\Psi}_R = \Psi_R\sqrt{R^3/N_*}$ versus radius $\tilde{r} = r/R$ in the modified Gaussian ansatz for different values of spherical harmonic number l.

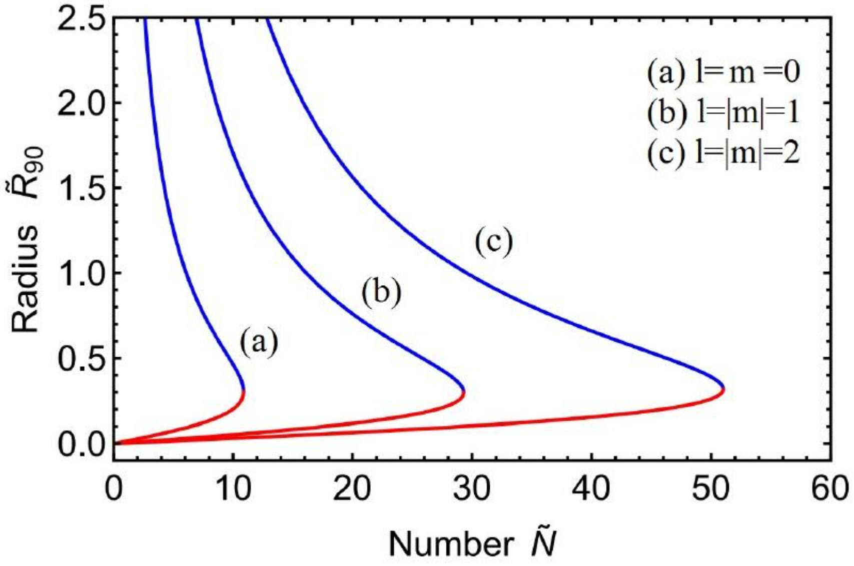

We plot R_{90} $(0.9N = 4\pi\int_0^{R_{90}} dr' r'^2\Psi(r')^2)$, where $\tilde{R}_{90} = m_\phi\delta^{1/2}R_{90}$ and $\tilde{N}_* = |\lambda|\delta^{1/2}N_*$.

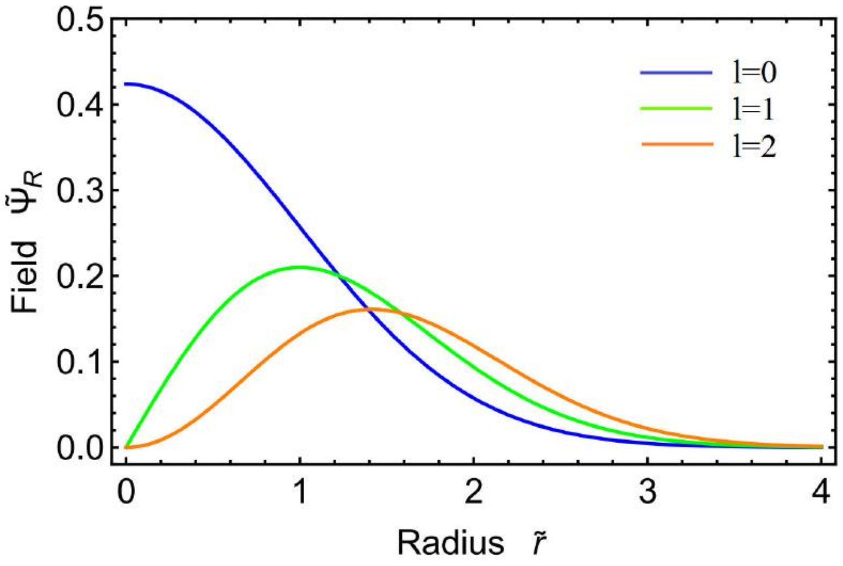

(Hertzberg and Schiappacasse, 2018)

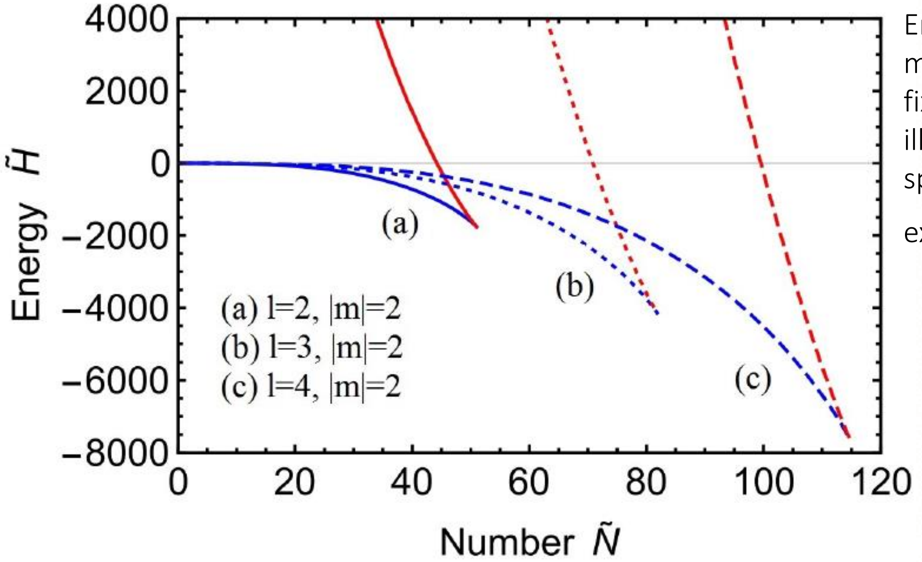

Energy of clump solution versus number with non-zero angular momentum parameter $|m| = 2$ for different values of l. At a fixed number N and angular momentum $L_z = Nm$, this illustrates that the configurations that minimizes the energy has spherical harmonic number $l = |m|$ (whenever the solution exists). Here $\tilde{H} = |\lambda|^{\frac{3}{2}}/(m_\phi^2\sqrt{G})H$ and $\tilde{N}_* = m_\phi\sqrt{G\,|\lambda|}$.

At high $l = |m|$,

$$N_{*,max} \approx \frac{10.52}{|\lambda|\sqrt{\delta}}\frac{(l^{3/2})}{(\ln l)^{1/4}} \; ; \; R_{min} \approx \frac{0.141}{m_\phi\sqrt{\delta}}\frac{(l^{1/2})}{(\ln l)^{1/4}}$$

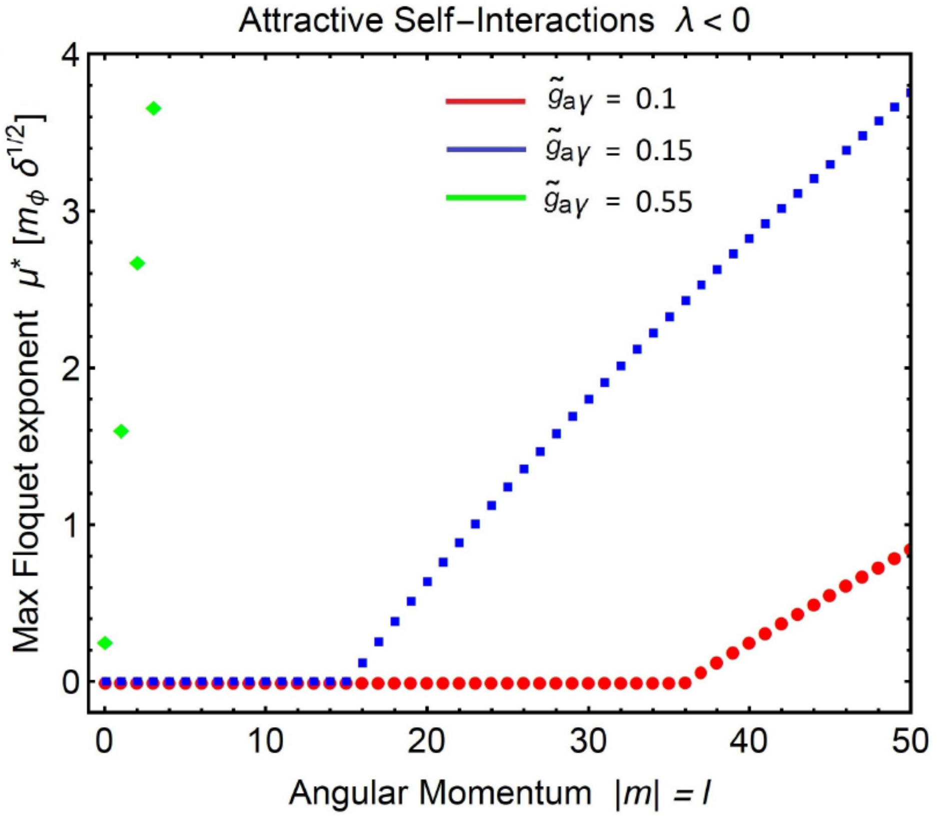

The maximum real part of Floquet exponent μ^*, describing parametric resonance of photons from a clump condensate as a function of its angular momentum $|m| = l$. We plot μ^* in units of $m_\phi\sqrt{\delta}$. This is for attractive self-interactions with $N_* = N_{*,max}$. Here $\tilde{g}_{a\gamma\gamma} = \frac{g_{a\gamma\gamma} f_a}{\sqrt{\gamma}}$.

$$\mu^* \approx Max(\mu_H^* - \mu_{esc}, 0)$$

The minimum axion-photon coupling $g_{a\gamma}$ that is necessary in order to have resonance from a clump condensate as a function of its angular momentum $|m| = l$. We plot in units of $\frac{\sqrt{\gamma}}{f_a}$. We take $N_* = N_{*,max}$.

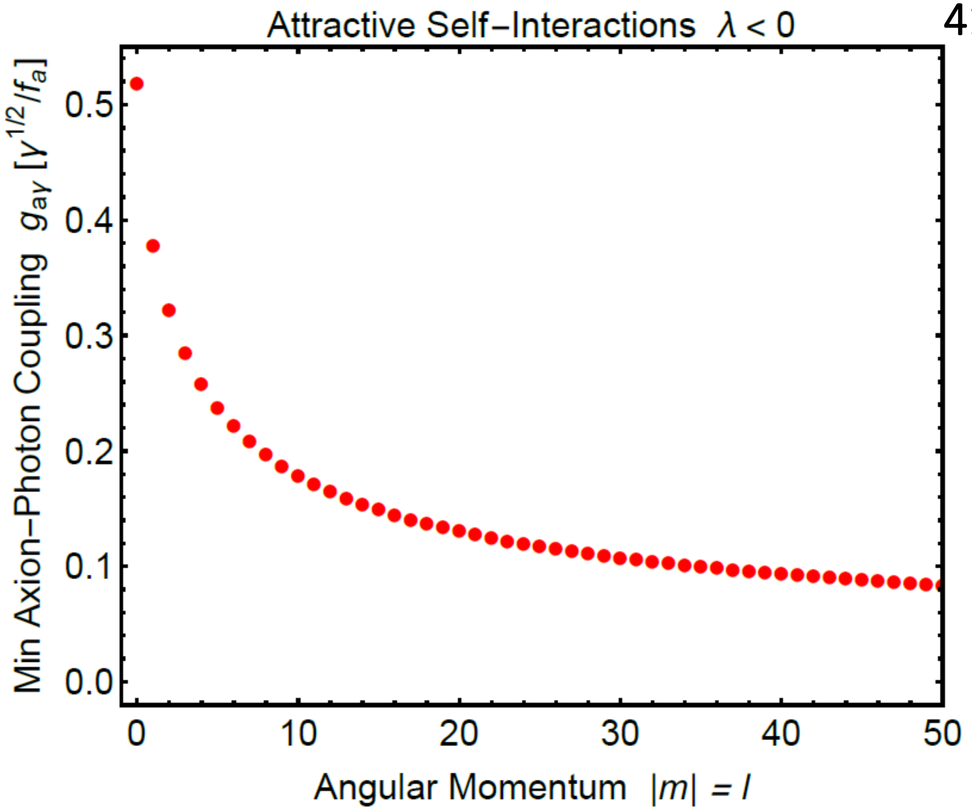

(Hertzberg and Schiappacasse, 2018)

By taking $\gamma = 0.3$ and $N_* = N_{*,max}$, for high angular momentum the minimum axion-photon coupling is just $g_{a\gamma\gamma} > g_{a\gamma\gamma,min} \approx \frac{\beta_c}{f_a\sqrt{l}}$ with $\beta_c = 0.3$

For the QCD axion $g_{a\gamma\gamma} = O(10^{-2})/f_a$, we need rather large angular momentum of $|m| = l \gtrsim O(10^3)$

REPULSIVE SELF-INTERACTIONS

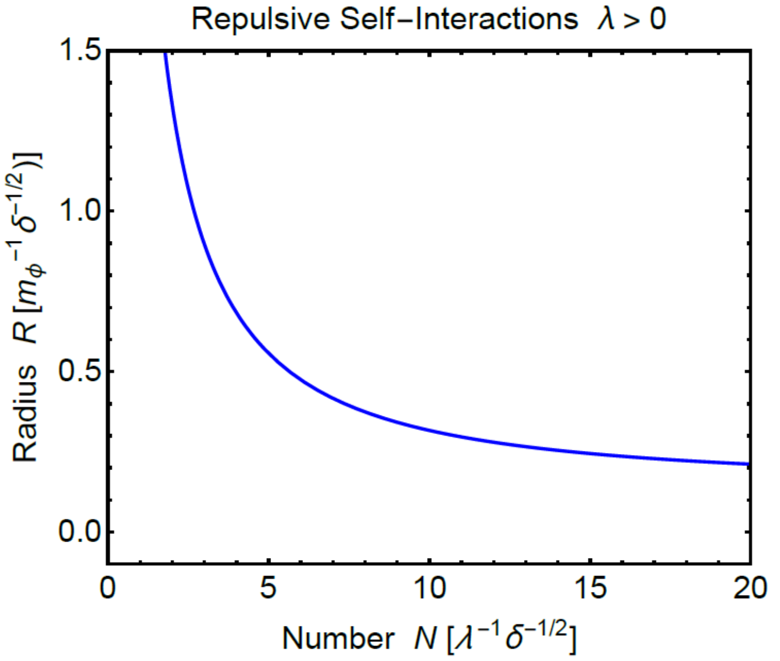

- For repulsive interactions we have only $\lambda > 0$ there is only 1 branch of solution. This branch is stable and there is no a maximum number of particles.

(Hertzberg and Schiappacasse, **1805.00430**)

The maximum real part of Floquet exponent μ^*, describing parametric resonance of photons from a spherically symmetric clump condensate, as a function of axion-photon coupling $g_{a\gamma\gamma}$. (Left) We plot μ^* in units of $m_\phi\sqrt{\delta}$, $g_{a\gamma\gamma}$ in units of $\frac{\sqrt{\gamma}}{f_a}$, and $\tilde{N}_* = N_*/(|\lambda|\sqrt{\delta})$. (Right) We plot μ^* in units of $m_\phi\sqrt{\delta}$ and N_*in units of $|\lambda|^{-1}\delta^{-1/2}$. Here $\tilde{g}_{a\gamma\gamma} = g_{a\gamma\gamma}f_a/\sqrt{\gamma}$.

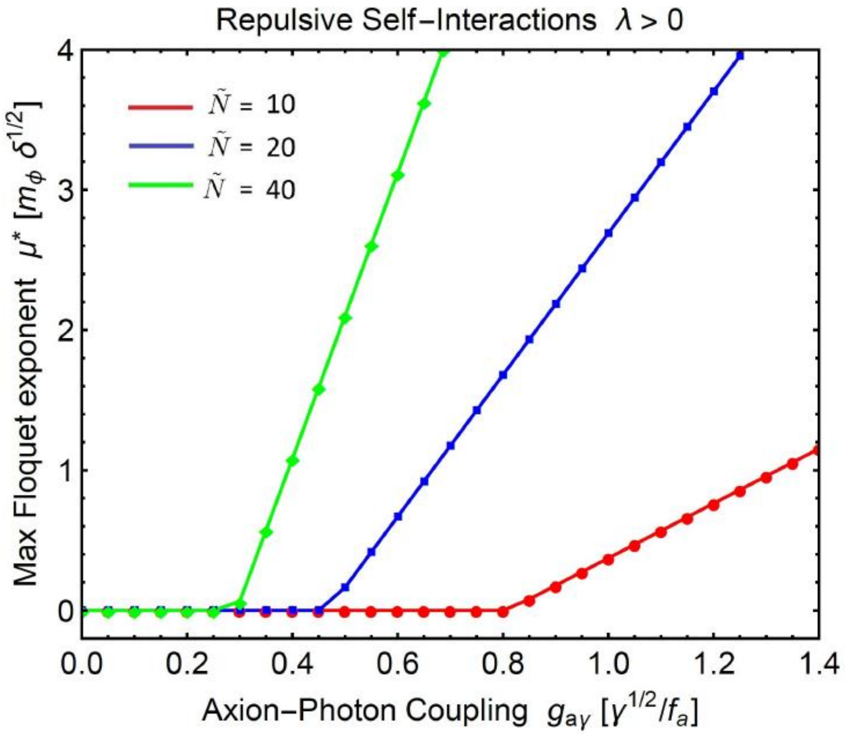

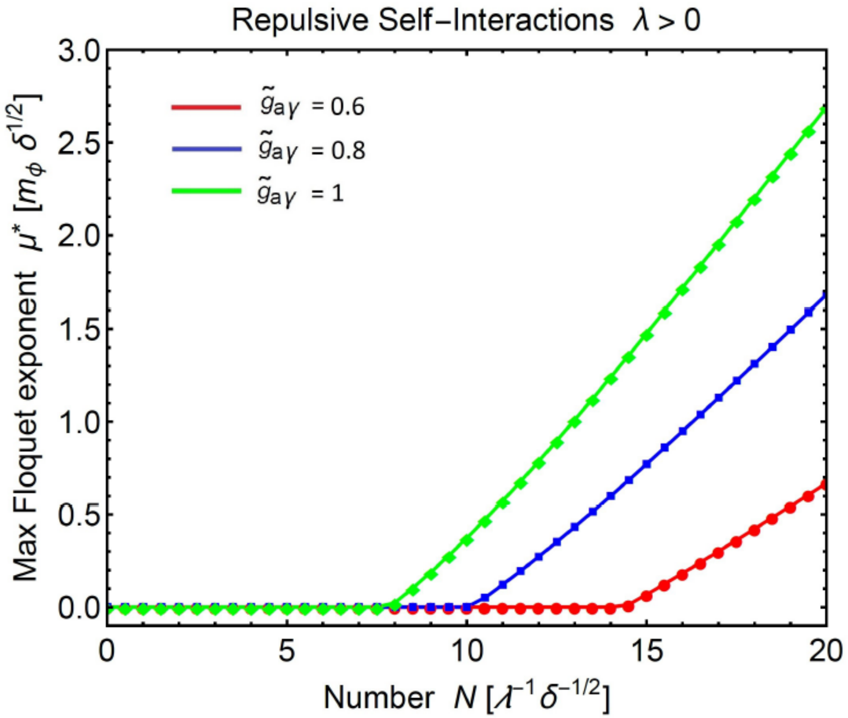

INTERFERENCE EFFECTS

$$\tilde{\psi}\left(\sqrt{\tilde{x}^2+\tilde{y}^2+(\tilde{z}+\tilde{z}_0)^2}\right)e^{i(\tilde{v}_{\tilde{z}}\tilde{z}+\tilde{\mu}\tilde{t})}+\tilde{\psi}\left(\sqrt{\tilde{x}^2+\tilde{y}^2+(\tilde{z}-\tilde{z}_0)^2}\right)e^{-i(\tilde{v}_{\tilde{z}}\tilde{z}-\tilde{\mu}\tilde{t}+\delta)}$$

$$|\tilde{\psi}(\tilde{\boldsymbol{x}},\tilde{t}_{int})|^2=2|\tilde{\psi}(\sqrt{\tilde{x}^2+\tilde{y}^2+\tilde{z}^2})|^2|1+\cos(2\check{v}_{\tilde{z}}\tilde{z}+\delta)|$$

- For a phase difference different to π clumps merge

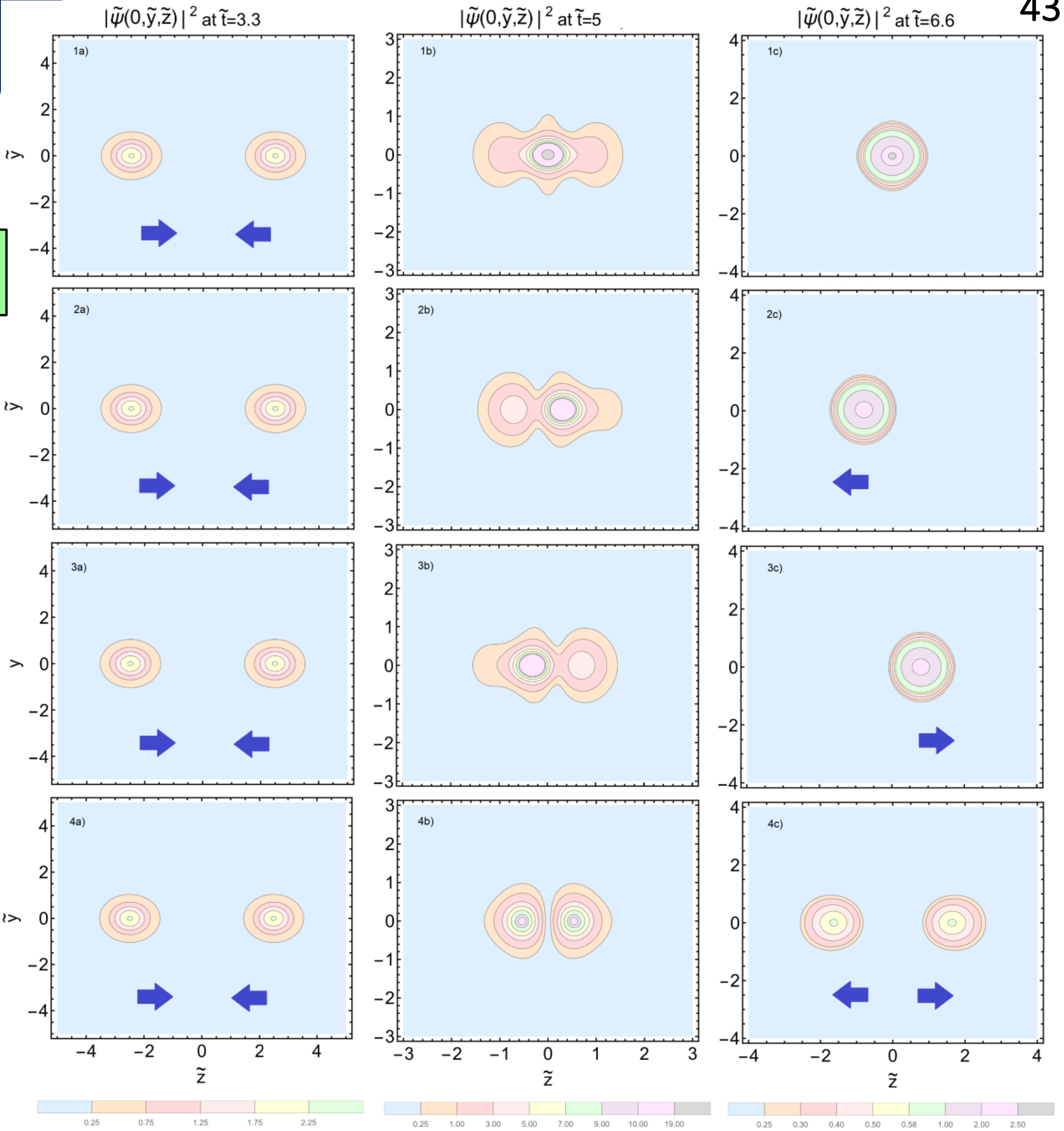

: Head-on collision between two clumps in their ground state configurations both with a number of particles $\tilde{N}_\star = 4.55418$ but different phase differences: $\delta = 0, \pi/2, 3\pi/2$ and π for the rows (1,2,3,4), respectively. For all cases, the center of mass of the two clumps are initially separated by a distance equal to $2\tilde{z}_0 = 12$ and have an initial velocity $\tilde{v}_{\tilde{z}} = 1$.

(Hertzberg, Li, Schiappacasse 2020)

NON-HEAD-ON COLLISIONS

(Hertzberg, Li, Schiappacasse 2020)

Non-head-on collision between two clumps that are originally in their ground state configurations; both with a number of particles $\tilde{N}_{\star} = 4.55418$. The center of mass of the two clumps are initially separated by a distance equal to $\sqrt{(2\tilde{z}_0)^2 + (2\tilde{x}_0)^2} = \sqrt{12^2 + 2^2}$ and have an initial velocity in the $\tilde{z}$-direction equal to $\tilde{v}_z = 0.5$.

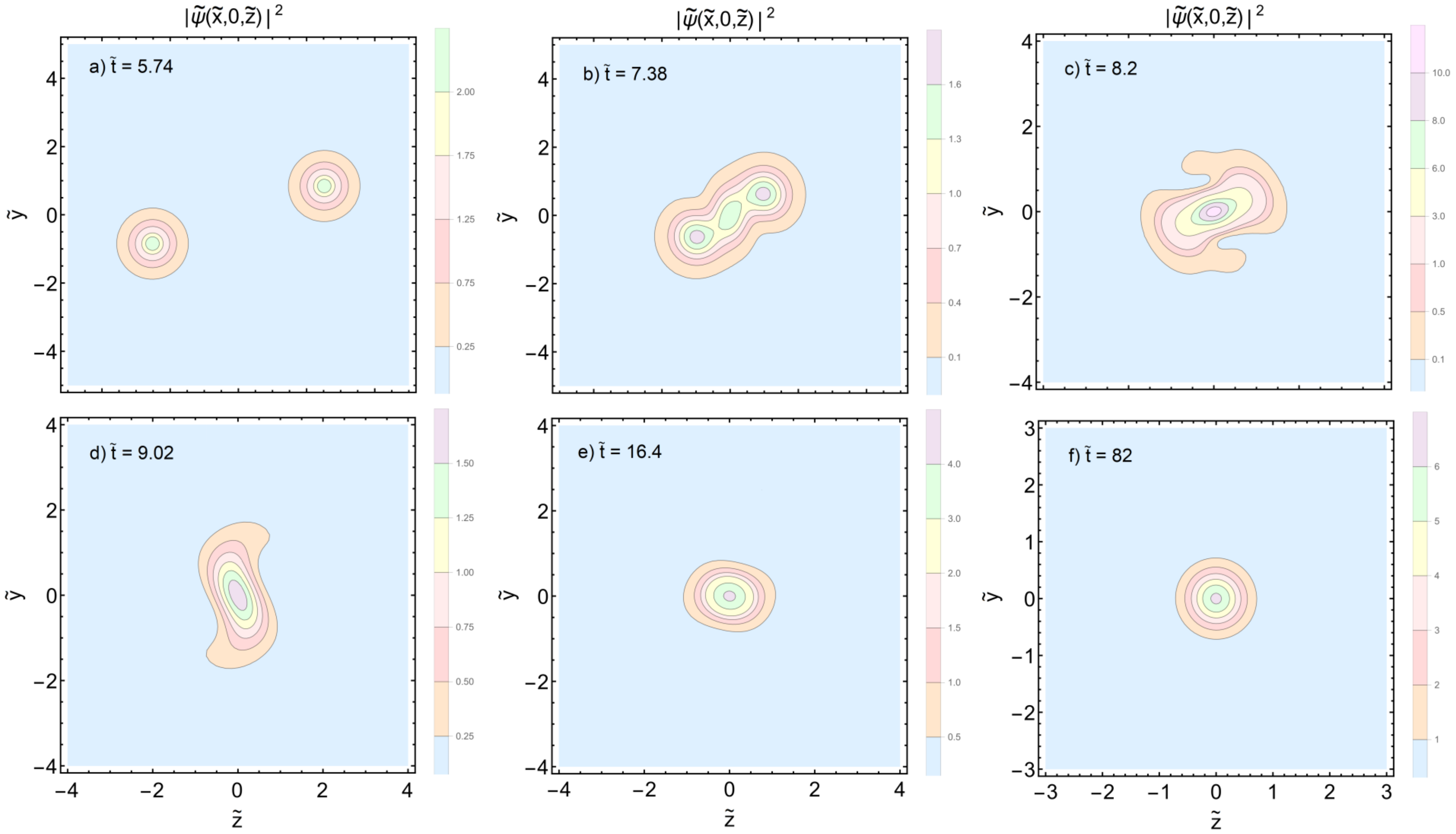

- The coalescence process takes longer in comparison to the head-on collision case.
- After merger , the process at which the resultant clump settle downs to the ground state by releasing the excess of particles is similar to those for the head-on collision case